ARCHIVES OF MECHANICS
Arch. Mech. **74** (4), 283–317, 2022, DOI: 10.24423/aom.4082

Bounds of the effective elastic moduli of nanoparticle-reinforced composites based on composite sphere assemblage and interface stress model

Z. TANG[1)], W. YE[1,2]

[1)] *College of Aerospace Engineering, Chongqing University, Chongqing 400044, China*

[2)] *Chongqing Key Laboratory of Heterogeneous Material Mechanics, Chongqing University, Chongqing 400044, China, e-mail: wye@cqu.edu.cn (corresponding author)*

Three different approaches are formulated to obtain the bounds of the effective elastic moduli of nanoparticle-reinforced composites based on the CSA and the interface stress model. It is found that the effective bulk modulus can be obtained by all three different approaches but the effective shear modulus can be obtained only by the energy approach. The bounds of the effective bulk modulus coincide and depend only on the interface bulk modulus, while those of the effective shear modulus are distinct and depend on two interface elastic constants. Furthermore, limit analysis discloses that the bounds of the effective bulk modulus of nanoparticles coincide but deviate from the bulk modulus of particle in the classical case, and the bounds of the effective shear modulus are distinct in contrast to the effective bulk modulus of nanoparticles or both effective moduli of conventional composites.

Key words: elastic moduli, bulk modulus, shear modulus, composite sphere assemblage, interface stress model.

1. Introduction

Particle-reinforced composites are widely used as structural and functional materials in engineering applications, where the effective elastic moduli of these materials are of great importance in the design process. Classical methods of predicting the effective elastic moduli of particle-reinforced composites may be divided into two categories: exact solutions and bound solutions. In exact solutions, most approaches are based on the famous Eshelby's single inclusion model [1], such as dilute concentration method [1], self-consistent method [2], Mori–Tanaka method [3] and double-inclusion method [4]. Moreover, such exact solutions depend in different ways on the elastic moduli, volume fraction, shape and orientation of the constituents, and some of them even take into considerations the spatial distribution of the constituents. In many cases, obtaining the exact solution to the effective elastic moduli of particle-reinforced composites

is a difficult task, while knowing the bounds is often enough in practical applications if the bounds are close enough. It is historically well-known that the least restrictive bounds are given as the Voigt upper and Reuss lower bounds due to the minimum potential and complementary energy theorems, respectively. However, these two bounds are too far apart to use, so more restrictive bounds are needed in practical situations. Hashin [5] proposed refined bounds of the effective elastic moduli of particle-reinforced composites based on the composite sphere assemblage (CSA) model, where the composite is assumed to be an assembly of composite spheres of various sizes. Similar bounds of the effective elastic moduli of fiber-reinforced composites were also derived based on a similar composite cylinder assemblage (CCA) model [6]. In CSA and CCA models, the spherical and cylindrical reinforcements are required to be distributed in a particular way. To remove this limitation, wider but more general bounds were proposed later as the Hashin–Shtrikman bounds [7]. It should be mentioned that the bounds based on CSA and CCA models are the most restrictive ones that can be given in terms of the volume fraction and elastic moduli of the constituents [8]. Therefore, they could be used to provide good estimates of the effective elastic moduli of composite materials in some practical situations.

However, interface property is not included in all the classical methods mentioned above, so they do not admit the size-dependence of the reinforcements. This is acceptable for conventional composites but would be inappropriate for nanocomposites because it has been disclosed that the behavior of nanomaterials could differ from conventional materials dramatically [9–13]. For example, in nanoparticle-reinforced composites, due to the large interface-to-volume ratio, interface effect begins to play an important role in changing the constitutive law seen in classical elasticity theory. To consider the interface effect, continuities/discontinuities of field quantities (displacement, stress or traction) are assumed to exist across the interface, which means four different types of interfaces could be considered [14]: perfect interfaces, cohesive interfaces, elastic interfaces and general interfaces. In classical methods, perfect interfaces are assumed as the reinforcement and matrix are ideally bonded, so both displacement and traction fields are continuous across the interface. For cohesive interfaces, the traction field is continuous but a displacement jump exists across the interface, and the displacement jump is related to the traction field at the interface. For instance, as a typical example of cohesive interfaces, Hashin [15] proposed the linear spring model where the displacement jump is proportional to the traction at the interface. On the contrary, for elastic interfaces, the displacement field is continuous but a traction jump exists across the interface. This means that the interface deforms coherently with the bulk materials in the vicinity of the interface, but the traction jump is related to an interface stress. Recently, generalized interfaces [16, 17] have been also investigated where both displacement and traction

jumps are assumed to exist across the interface, and aforementioned cohesive and elastic interfaces are only two limit cases of the generalized interfaces.

In this work, elastic interfaces are considered because the interest in this subject has intensified in recent years for its importance in the properties of nanomaterials. As mentioned above, the traction jump is related to an interface stress for an elastic interface, so interface stress model should be proposed to determine the behavior of the elastic interface. Due to the similarity between surfaces and interfaces, surface/interface stress models are historically discussed interchangeably. SHUTTLEWORTH [18] first described the surface effect as a relationship of the deformation-dependent surface energy with the surface stress. GURTIN and MURDOCH [19] linked the surface/interface stress to the bulk stress in the vicinity of the surface/interface by regarding it as a negligibly thin object adhering to the underlying material without slipping. MILLER and SHENOY [20] introduced the concept of surface stiffness and demonstrated size-dependent elastic property of nano-sized structure members. DINGREVILLE *et al.* [21, 22] proposed to formulate the surface/interface excess energy as a quadratic function of the surface/interface strain where a group of intrinsic surface/interface property tensors could be defined. Based on the interface stress model, some exact solutions to the effective elastic moduli of nanoparticle-reinforced composites are obtained. SUN *et al.* [23] investigated the interface effect on the effective elastic property of nanoparticle-reinforced composites based on the CSA model, but only the effective bulk modulus was considered. CHEN *et al.* [24] derived the effective bulk modulus of nanoparticle-reinforced composites with an interface effect based on the construction of neutral composite spheres [25], which is an analogous type of the CSA model. Meanwhile, the effective shear modulus was obtained based on the generalized self-consistent method (GSCM) [26]. DUAN *et al.* [27] formulated a micromechanical framework of obtaining the effective moduli of solids containing nano-inhomogeneity with the interface effect by a strain concentration tensor inside the inhomogeneity and another strain concentration tensor at the interface. The effective bulk modulus was obtained in conjunction with CSA, GSCM and Mori–Tanaka method while the effective shear modulus was obtained in conjunction with the GSCM and Mori–Tanaka method.

Meanwhile, it is worthwhile to mention that an alternative approach to account for the interface effect in nanocomposites is to treat the interface as an interphase, which is the interfacial region defined by the narrow volume sandwiched between two bulk materials. For a thin and compliant interphase, the differences in the displacement and stress fields across the interphase have the same features with those of the linear spring interface model [28]. On the other hand, for a thin and stiff interphase, the differences in the displacement and stress fields across the interphase have the same features with those of the interface

stress model [29]. Therefore, the equivalence between interphase and interface effects on the effective elastic moduli of nanocomposites is assured when the link of the properties between interface and interphase is provided [30]. When the interface is treated as an interphase, the determination of the effective elastic moduli of particle-reinforced composites becomes the coated or multi-coated inclusion problem [31, 32] where all the interfaces between the interphase and other phases are regarded as perfect interfaces. Furthermore, one can even consider the interfaces as imperfect to derive the effective properties of multi-coated-inclusion composites with the imperfect interface effect. For instance, Hervé-Luanco [33, 34] proposed a new transfer matrix procedure with GSCM to obtain the effective elastic moduli of n-layered inclusion based composites with the imperfect interface effect. Pham *et al.* [35] obtained the effective elastic moduli of multi-coated-inclusion composites with the imperfect interface effect from the minimum energy principles and near-interaction approximations following previous investigations on the effective thermal and electrical properties [36, 37].

However, bound solutions are quite rare in the literature about the effective elastic moduli of nanoparticle-reinforced composites by considering the interface effect based on the interface stress model. After the seminal Hashin's CSA bounds and Hashin-Shtrikman bounds of the effective elastic moduli of particle-reinforced composites, tighter bounds [38–40] were constructed by considering the microgeometries of composites with additional statistical information. Besides the elastic properties and volume fractions of the component materials, these tighter bounds contained the three-point correlation parameters involving integrals of infinite medium Green's functions, which extended the bound solutions from two-component to multi-component composites. Unfortunately, the interface effect is not considered in all these bound solutions so they are still only applicable to conventional composites. As far as the authors have found in the literature, bound solutions to the effective elastic moduli of nanoparticle-reinforced composites were only reported by Firooz *et al.* [16] and again included in their recent review [41] based on Hashin's CSA model by considering the general interface effect. However, their bound solutions were mainly used for comparisons with exact solutions without deep insight into the bounds themselves.

This work investigates the bounds of the effective elastic moduli of nanoparticle-reinforced composites based on the CSA and the interface stress model. It should be noted that the general interface model deals with the traction jump in the same way with the interface stress model, and the additional displacement jump could be tackled similarly and less complicated mathematically than the traction jump. Therefore, only the interface stress model is used in this wok but it can be extended to the general interface model using similar strategies. Since the interface stress model is the most popular and widely used in the literature for the past decades, the fully explicit results in this work could be easier to use

for other studies compared with the results presented as implicit equations in other reports [16, 41]. This work is organized as follows. In Section 2, the solution to the elastic field is elaborated as the boundary value problem in the theory of elasticity based on the CSA and interface stress model, which is then used to derive the bounds of the effective elastic moduli by three different approaches. Closed-form solutions are presented in Section 3 as well as the validations with other theoretical and experimental results. In Section 4, the influences of interface effect and size of nanoparticles on the bounds of the effective elastic moduli of nanoparticle-reinforced composites are discussed in detail. The limit analysis is performed on the bounds of the effective elastic moduli of nanoparticle-reinforced composites when the particle concentration is extremely small or large. Some unexpected results are found which may be unnoted in the literature.

2. Methodology

For completeness, the concept of Hashin's CSA model is reviewed briefly with the consideration of interface effect. The elastic field is formulated as the boundary value problem in the theory of elasticity based on the CSA and the interface stress model, which is then used to derive the bounds of the effective elastic moduli by three different approaches.

2.1. Composite sphere assemblage (CSA) model

In Fig. 1a, the nanoparticle-reinforced composite is composed of an isotropic matrix in which isotropic nano-sized spherical inhomogeneity is embedded. According to the CSA model, the original composite could be constructed by filling it with composite sphere elements which may diminish to an infinitesimal size such that no matrix volume is left between the outer surfaces of composite sphere elements. A typical composite sphere element is represented in Fig. 1b by a spherical inhomogeneity of radius a concentric with a spherical matrix shell of the outer radius b. The volumes of the inhomogeneity and matrix are V_i and V_m, respectively. The interface between inhomogeneity and matrix is denoted by Γ. For all composite sphere elements, the local volume fraction of inhomogeneity is the same, which equals to the global volume fraction of the reinforcements inside the original composite as $f = (a/b)^3$. In this case, the outer radius b in Fig. 1b is just an imaginary boundary and it should not enter the final solution to the effective elastic moduli of nanoparticle-reinforced composites. It follows that the particle-reinforced composite is macroscopically isotropic and the effective elastic moduli are the same with those of each composite sphere element [5]. Therefore, the derivations are directly performed on the composite sphere element for convenience in the following.

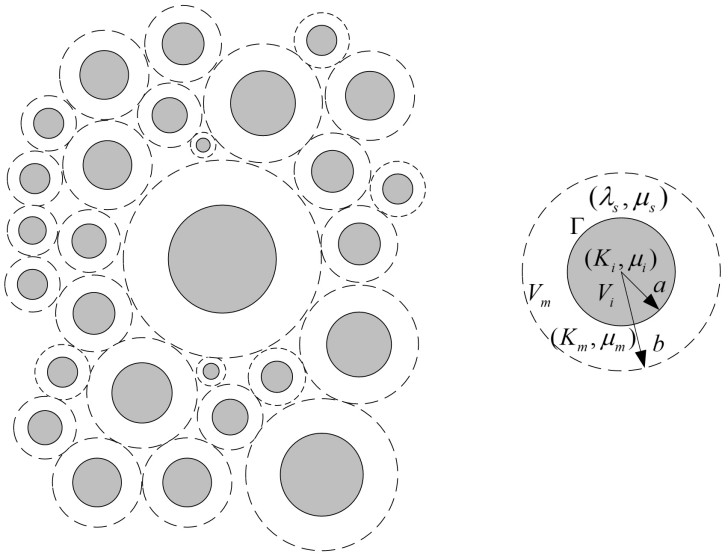

a) b)

FIG. 1. Composite sphere assemblage model of the nanoparticle-reinforced composite; a) composite sphere assemblagem b) composite sphere element.

2.2. Field equations

In the composite sphere element, both the matrix and inhomogeneity are assumed to be isotropic materials. Therefore, the constitutive relationship between the stress and strain field is:

$$\sigma_{ij} = C_{ijkl}\varepsilon_{kl} = \lambda\varepsilon_{kk}\delta_{ij} + 2\mu\varepsilon_{ij}, \tag{2.1}$$

where C_{ijkl} is the stiffness tensor and $C_{ijkl} = \lambda\delta_{ij}\delta_{kl} + \mu(\delta_{ik}\delta_{jl} + \delta_{il}\delta_{jk})$ in the isotropic case with Lamé constants, λ and μ; δ_{ij} is the Kronecker delta. The second Lamé constant μ is also called the shear modulus, and the bulk modulus is given as $K = \lambda + 2\mu/3$. In the following, the elastic moduli of the matrix and inhomogeneity are denoted as (K_m, μ_m) and (K_i, μ_i), respectively.

From continuum mechanics, the stress field in both the matrix and inhomogeneity is governed by the stress equilibrium condition without body forces as:

$$\sigma_{ij,j} = 0. \tag{2.2}$$

Under small deformation hypothesis, the geometric relationship in both the matrix and inhomogeneity between the displacement and strain field is:

$$\varepsilon_{ij} = \tfrac{1}{2}(u_{i,j} + u_{j,i}). \tag{2.3}$$

Combining Eqs. (2.1)–(2.3), the displacement field in both the matrix and inhomogeneity satisfies the following Lamé–Navier equation as:

$$\mu u_{i,jj} + (\lambda + \mu) u_{j,ji} = 0. \tag{2.4}$$

For convenience, Eq. (2.4) can be also written as:

$$(1 - 2\nu) u_{i,jj} + u_{j,ji} = 0, \tag{2.5}$$

where ν is Poisson's ratio. In the following, Poisson's ratios of the matrix and inhomogeneity are denoted as ν_m and ν_i, respectively.

2.3. Boundary conditions

The field equations aforementioned describe the relationships of the field quantities (displacement, stress and strain) in the whole domain. To solve the problem, boundary conditions should be appended, which concern the field quantities at the interface between the matrix and inhomogeneity ($r = a$), and the external surface of the matrix shell ($r = b$), respectively.

2.3.1. Interface stress model. Since the critical length of nanoparticles drops down to several nanometers, the mechanical behavior of the interface between the matrix and inhomogeneity should be considered to be size-dependent. In the interface stress model, the linear constitutive relationship between interface stress and interface strain is given as [19, 20]:

$$\sigma^s_{\alpha\beta} = \sigma^0_{\alpha\beta} + C^s_{\alpha\beta\gamma\delta}\varepsilon^s_{\gamma\delta} = \sigma^0_{\alpha\beta} + \lambda_s \varepsilon^s_{\gamma\gamma}\delta_{\alpha\beta} + 2\mu_s \varepsilon^s_{\alpha\beta}, \tag{2.6}$$

where $\sigma^0_{\alpha\beta}$ is the residual interface stress when the bulk materials are unstrained and it is usually neglected [24, 27]; $C^s_{\alpha\beta\gamma\delta}$ is the interface stiffness tensor and $C^s_{\alpha\beta\gamma\delta} = \lambda_s \delta_{\alpha\beta}\delta_{\gamma\delta} + \mu_s(\delta_{\alpha\gamma}\delta_{\beta\delta} + \delta_{\alpha\delta}\delta_{\beta\gamma})$ in the isotropic case; λ_S and μ_S could be regarded as interface Lamé constants and the interface bulk modulus can be defined as $K_s = \lambda_s + \mu_s$.

Additionally, the interface between the matrix and inhomogeneity is considered to deform coherently without slipping from the bulk material. In this case, the interface strain equals to the bulk strain so the displacement and strain field are continuous across the interface. However, the bulk stress field in the matrix and inhomogeneity are discontinuous and it is determined from the interface stress in the vicinity of the interface as [19, 20]:

$$\sigma^s_{\alpha\beta,\beta} + \langle\langle \sigma_{\alpha j} n_j \rangle\rangle = 0, \tag{2.7}$$

$$\sigma^s_{\alpha\beta}\kappa_{\alpha\beta} = \langle\langle \sigma_{ij} n_i n_j \rangle\rangle, \tag{2.8}$$

where n_i is the unit vector normal to the interface; $\kappa_{\alpha\beta}$ is the interface curvature tensor and $\langle\langle * \rangle\rangle = (*)_m - (*)_i$ denotes the quantity jump across the interface from the inhomogeneity to matrix.

It should be noted that the interface stress tensor is a two-dimensional quantity and the strain normal to the interface is excluded. Thus, the Greek indices take the value of 1 or 2, while Latin subscripts adopt values from 1 to 3. Eq. (2.7) could be regarded as an interface stress equilibrium equation similar to the bulk stress equilibrium equation of Eq. (2.2), while Eq. (2.8) could be regarded as the interface boundary condition.

2.3.2. External surface. Finally, the elastic field in the composite sphere element could be determined by subjecting the external surface of the matrix shell to either displacement or traction boundary condition as:

$$u_i^{(0)} = \varepsilon_{ij}^0 x_j, \tag{2.9}$$

$$t_i^{(0)} = \sigma_{ij}^0 n_j, \tag{2.10}$$

where ε_{ij}^0 and σ_{ij}^0 are constant tensors.

Generally, the upper bound of the effective elastic moduli of the composite sphere element is obtained by applying displacement boundary condition on the outer radius of the element, while the lower bound is obtained by applying a traction boundary condition.

More specifically, according to the CSA model, the composite sphere element is isotropic with bulk modulus of $\bar{K}$ and shear modulus of $\bar{\mu}$. To obtain the effective bulk modulus, the spherically symmetric boundary condition should be applied on the external surface of the matrix shell, so Eqs. (2.9) and (2.10) are reduced to:

$$u_i^{(0)} = \varepsilon^0 x_i, \tag{2.11}$$

$$t_i^{(0)} = \sigma^0 n_i, \tag{2.12}$$

where ε^0 and σ^0 are constant scalars.

Similarly, to obtain the effective shear modulus, the transverse shear boundary condition should be applied on the external surface of the matrix shell, so Eqs. (2.9) and (2.10) are reduced to:

$$u_1^{(0)} = \frac{\gamma^0}{2} x_2, \quad u_2^{(0)} = \frac{\gamma^0}{2} x_1, \quad u_3^{(0)} = 0, \tag{2.13}$$

$$t_1^{(0)} = \tau^0 n_2, \quad t_2^{(0)} = \tau^0 n_1, \quad t_3^{(0)} = 0, \tag{2.14}$$

where γ^0 and τ^0 are constant scalars.

2.4. Elastic field

Based on the CSA and the interface stress model above, the elastic field is solved as the boundary value problem in the theory of elasticity by combining the field equations in Section 2.2 and boundary conditions in Section 2.3.

2.4.1. Spherically symmetric boundary condition. When spherically symmetric displacement or traction boundary condition of Eq. (2.11) or (2.12) is applied on the external surface of the matrix shell, the displacement field is spherically symmetric, so the only nonzero displacement component in a spherical coordinate system is the radial displacement $u_r = u_r(r)$. From Eq. (2.5), the displacement field in both the matrix and inhomogeneity takes the following form as:

$$u_r = Ar + \frac{B}{r^2}, \tag{2.15}$$

where the unknown constants are determined through boundary conditions in Section 2.3.

With the displacement field given above, the strain and stress field in both the matrix and inhomogeneity could be found easily afterwards. Therefore, all the elastic field has been obtained for spherically symmetric boundary conditions.

2.4.2. Transverse shear boundary condition. When transverse shear boundary condition is applied on the external surface of the matrix shell, the displacement field in both the matrix and inhomogeneity takes the following form as:

$$\begin{aligned} u_r &= U_r(r)\sin^2\theta\cos 2\phi, \\ u_\theta &= U_\theta(r)\sin\theta\cos\theta\cos 2\phi, \\ u_\phi &= U_\phi(r)\sin\theta\sin 2\phi, \end{aligned} \tag{2.16}$$

where U_r, U_θ, U_ϕ are unknown functions of only r.

From Eq. (2.5), the three unknown functions satisfy the following relationships:

$$\begin{aligned} &2(1-\nu)U_r'' + \frac{4(1-\nu)}{r}U_r' - \frac{3U_\theta'}{r} + \frac{9-12\nu}{r^2}U_\theta + \frac{16\nu-10}{r^2}U_r = 0, \\ &(1-2\nu)U_\theta'' + \frac{2(1-2\nu)}{r}U_\theta' + \frac{2}{r}U_r' + \frac{8(1-\nu)}{r^2}U_r - \frac{12(1-\nu)}{r^2}U_\theta = 0, \\ &U_\theta + U_\phi = 0. \end{aligned} \tag{2.17}$$

The solution takes the following form:

$$
\begin{aligned}
U_r &= A_1 r - \frac{6\nu}{1-2\nu} A_2 r^3 + \frac{3A_3}{r^4} + \frac{A_4(5-4\nu)}{(1-2\nu)r^2}, \\
U_\theta &= A_1 r - \frac{7-4\nu}{1-2\nu} A_2 r^3 - \frac{2A_3}{r^4} + \frac{2A_4}{r^2}, \\
U_\phi &= -U_\theta,
\end{aligned}
\tag{2.18}
$$

where the unknown constants are determined through boundary conditions in Section 2.3 and they are too cumbersome to be listed here. When the displacement field is solved, the strain and stress field in both the matrix and inhomogeneity could be found easily afterwards. Therefore, all the elastic field has been obtained for transverse shear boundary conditions.

2.5. Effective elastic moduli

The basic idea to obtain the effective elastic moduli of the nanoparticle-reinforced composites is to compare certain quantities of the composite sphere element with that of a homogeneous equivalent medium with the unknown effective elastic moduli under the same boundary conditions. Here we chose the quantity as the strain energy, average stress and strain, and boundary responses on the outer surface (traction or displacement vector), respectively. Each approach has been used in the literature for the calculation of either the effective bulk or shear modulus of composites, but no explanation is made about the applicability (and reason) of each approach to either effective modulus, which is investigated with discussions on the cons and pros of each approach in the following.

2.5.1. Energy approach. The approach to obtain the effective elastic moduli is based on the variational principle by equating the strain energy of the composite sphere element to a homogeneous equivalent medium with unknown stiffness $\bar{C}_{ijkl}$. This approach was first proposed by HASHIN [5] to obtain the bounds of the effective elastic moduli of composites as the classical solution where no interface effect was considered. Based on the interface stress model, this approach has been adopted by CHEN *et al.* [24] to obtain the exact solution to the effective shear modulus by the generalized self-consistent method.

When the displacement boundary condition of Eq. (2.9) is applied, the strain field in the homogeneous medium is simply ε^0_{ij} and the stress field is $\bar{C}_{ijkl}\varepsilon^0_{kl}$ so the strain energy in the homogeneous equivalent medium can be written as:

$$
U_h = \frac{1}{2} \int_V \overline{C}_{ijkl} \varepsilon^0_{ij} \varepsilon^0_{kl} \, dV. \tag{2.19}
$$

When the traction boundary condition of Eq. (2.10) is applied, the stress field in the homogeneous medium is simply σ_{ij}^0 and the strain field is $(\bar{C}_{ijkl})^{-1}\sigma_{kl}^0$ so the strain energy in the homogeneous equivalent medium can be written as:

$$U_h = \frac{1}{2}\int_V (\overline{C}_{ijkl})^{-1}\sigma_{ij}^0\sigma_{kl}^0\, dV. \tag{2.20}$$

For the heterogeneous composite sphere element, the total strain energy is contributed by the inhomogeneity, matrix and interface together as:

$$U_c = U_i + U_m + U_\Gamma, \tag{2.21}$$

where

$$U_i = \frac{1}{2}\int_{V_i} \sigma_{ij}^i\varepsilon_{ij}^i\, dV, \tag{2.22}$$

$$U_m = \frac{1}{2}\int_{V_m} \sigma_{ij}^m\varepsilon_{ij}^m\, dV, \tag{2.23}$$

$$U_\Gamma = \frac{1}{2}\int_\Gamma \sigma_{\alpha\beta}^S\varepsilon_{\alpha\beta}^S\, d\Gamma. \tag{2.24}$$

A direct calculation of Eq. (2.21) involves cumbersome volume integrals of quadratic terms, which need to be rewritten into a simpler form by using the perturbation method proposed by ESHELBY [42]:

$$U_c = U_0 + \delta U, \tag{2.25}$$

where U_0 is the strain energy of a uniform matrix without the inhomogeneity subjected to the same boundary condition by replacing $\bar{C}_{ijkl}$ with $C_{ijkl}^{(m)}$ in Eqs. (2.19) and (2.20).

When displacement boundary condition of Eq. (2.9) is applied, the perturbing strain energy is given as:

$$\delta U = \frac{1}{2}\int_\Gamma (t_i^{(\Gamma)}u_i^{(0)} - t_i^{(0)}u_i^{(\Gamma)})\, d\Gamma, \tag{2.26}$$

where $u_i^{(\Gamma)}$ and $t_i^{(\Gamma)}$ are the displacement and traction at the interface respectively.

When the traction boundary condition of Eq. (2.10) is applied, the perturbing strain energy is given as:

$$\delta U = -\frac{1}{2}\int_\Gamma (t_i^{(\Gamma)}u_i^{(0)} - t_i^{(0)}u_i^{(\Gamma)})\, d\Gamma. \tag{2.27}$$

In Eqs. (2.26) and (2.27), since the interface is considered to deform coherently, then $u_i^{(\Gamma)} = u_i^{\mathrm{i}} = u_i^{\mathrm{m}}$ so one can use either u_i^{i} or u_i^{m} for $u_i^{(\Gamma)}$ However, stress discontinuity exists at the interface of the composite sphere element, one must use the stress field in the matrix to calculate $t_i^{(\Gamma)} = \sigma_{ij}^{\mathrm{m}} n_j$. This is in contrast to the original perturbation method proposed by Eshelby for perfectly bonded interfaces of heterogeneous materials where $t_i^{(\Gamma)} = \sigma_{ij}^{\mathrm{m}} n_j = \sigma_{ij}^{\mathrm{i}} n_j$.

By equating Eq. (2.25) to Eq. (2.19) and Eq. (2.20), i.e., if the strain energy of the composite sphere element is considered to be the same with that of a homogeneous equivalent medium, the upper and lower bounds of the effective elastic moduli of nanoparticle-reinforced composites could be obtained, respectively.

2.5.2. Average approach. A straightforward approach to obtain the effective elastic moduli is expressed by the average stress and strain tensors:

$$\overline{\sigma}_{ij} = \overline{C}_{ijkl}\overline{\varepsilon}_{kl}, \tag{2.28}$$

where the overbar denotes the volume average; $\bar{C}_{ijkl}$ is the effective stiffness tensor and $\bar{C}_{ijkl} = \bar{K}\delta_{ij}\delta_{kl} + \bar{\mu}(\delta_{ik}\delta_{jl} + \delta_{il}\delta_{jk} - 2\delta_{ij}\delta_{kl}/3)$ in the isotropic case.

In this approach, the effective elastic moduli are obtained by equating the average stress and strain in the composite sphere element to those of a homogeneous medium of the same size with unknown stiffness $\bar{C}_{ijkl}$, which is to be solved by Eq. (2.28). It should be mentioned that, for general imperfect interfaces, the volume average of the composite should be carried out by considering the discontinuities of displacement or stress field across the interface. Based on the interface stress model, the average strain and stress tensors are given as [43]:

$$\overline{\varepsilon}_{ij} = f\overline{\varepsilon_{ij}^{i}} + (1-f)\overline{\varepsilon_{ij}^{m}}, \tag{2.29}$$

$$\overline{\sigma}_{ij} = f\overline{\sigma_{ij}^{i}} + (1-f)\overline{\sigma_{ij}^{m}} + \frac{f}{V}\int_{\Gamma} \langle\langle \sigma_{ik} \rangle\rangle n_k x_j \, d\Gamma, \tag{2.30}$$

where displacement discontinuity is not included because the interface is considered to deform coherently, but the stress jump across the interface exists according to the interface stress model.

The average approach involves volume integrals of the stress and strain fields in the inhomogeneity and matrix respectively, and a surface integral of the stress jump at the interface. These integrals are tackable for the spherically symmetric boundary condition in Eqs. (2.11) or (2.12) to determine the effective bulk modulus. However, for the transverse shear boundary condition, with the displacement field given with trigonometric functions in Eq. (2.16), the stress and strain field will also be trigonometric functions, so the volume integrals of the stress and strain field will be both zero. Therefore, arbitrary effective shear modulus satisfies Eq. (2.28), so it could not be determined by this approach.

2.5.3. Boundary approach. When the displacement boundary condition is applied, a stress field will be generated in the whole domain of the composite and the traction vector can be calculated at the outer shell of the matrix. Under the same displacement boundary condition, the traction vector for a homogeneous medium of the same size also can be calculated at the boundary. A proper effective elastic moduli of the composite should guarantee these two traction vectors be equal to each other naturally. Therefore, this approach obtains the effective elastic moduli by equating the traction response on the outer surface of the composite sphere element to that of a homogeneous sphere of the same size as the composite sphere element under the same displacement boundary condition. Similarly, when the traction boundary condition is applied, this approach obtains the effective elastic moduli by equating the displacement response on the outer surface of the composite sphere element to that of a homogeneous sphere of the same size under the same traction boundary condition. Since the elastic field solution has been obtained in Section 2.4, the traction or displacement solution on the outer surface could be used directly to compare with that of a homogeneous sphere of the same size under the same boundary condition. The advantage of this approach is that, neither volume nor surface integral is involved in this approach, and only simple algebraic calculations are needed to obtain the effective elastic moduli. Based on the interface stress model, this approach has been adopted by CHEN *et al.* [24] to obtain the effective bulk modulus of nanoparticle-reinforced composites. However, it should be noted that the quantity to be compared in the composite sphere element and that of a homogeneous sphere is the traction or displacement vector on the outer surface, i.e., a vector-form quantity should be compared in this approach. Therefore, all components of the vector-form quantity should be satisfied simultaneously with no conflicts. Unfortunately, as it is seen in Section 3, the effective bulk modulus could be obtained by this approach but it fails to obtain the effective shear modulus.

3. Results

In this section, closed-form solutions to the effective elastic moduli of nanoparticle-reinforced composites is provided based on the CSA and interface stress models. Comparison with experiment results is presented afterwards.

3.1. Effective bulk modulus

When spherically symmetric displacement or traction boundary condition of Eq. (2.11) or (2.12) is applied on the external surface of the matrix shell, the elastic field (displacement, strain and stress) in both the matrix and inhomogeneity has been found in Section 2.4.1. Afterwards, according to Section 2.5, the effec-

tive bulk modulus of the nanoparticle-reinforced composites could be obtained by comparing the strain energy, average stress and strain, and the boundary response, respectively, of the composite sphere element with that of a homogeneous equivalent medium with the unknown effective elastic moduli under the same boundary conditions.

Following the energy approach in Section 2.5.1, the strain energy of the composite sphere element can be calculated by Eq. (2.25), which is compared with the strain energy of a homogeneous equivalent medium to obtain the bounds of the effective bulk modulus. Similar to the classical case without the consideration of the interface effect, the upper and lower bounds of the effective bulk moduli of nanoparticle-reinforced composites coincide as given below:

$$\overline{K}_{upper} = \overline{K}_{lower} = K_m + \frac{f\left(K_i - K_m + \frac{4K_s}{3a}\right)}{1 + (1-f)\left(\frac{K_i - K_m}{K_m + \frac{4}{3}\mu_m}\right) + \frac{4K_s}{3a\left(K_m + \frac{4}{3}\mu_m\right)}}. \tag{3.1}$$

Following the average approach in Section 2.5.2, the average strain and stress field of the composite sphere element can be calculated by Eqs. (2.29) and (2.30), which is compared with that of a homogeneous equivalent medium to obtain the bounds of the effective bulk modulus. For convenience, Eq. (2.28) is rewritten in a matrix form under the spherical coordinate system as:

$$\begin{pmatrix} \overline{\sigma}_{rr} \\ \overline{\sigma}_{\theta\theta} \\ \overline{\sigma}_{\phi\phi} \\ \overline{\sigma}_{r\theta} \\ \overline{\sigma}_{r\phi} \\ \overline{\sigma}_{\theta\phi} \end{pmatrix} = \begin{pmatrix} \overline{K} + \frac{4}{3}\overline{\mu} & \overline{K} - \frac{2}{3}\overline{\mu} & \overline{K} - \frac{2}{3}\overline{\mu} & & & \\ \overline{K} - \frac{2}{3}\overline{\mu} & \overline{K} + \frac{4}{3}\overline{\mu} & \overline{K} - \frac{2}{3}\overline{\mu} & & 0 & \\ \overline{K} - \frac{2}{3}\overline{\mu} & \overline{K} - \frac{2}{3}\overline{\mu} & \overline{K} + \frac{4}{3}\overline{\mu} & & & \\ & & & 2\overline{\mu} & & \\ & 0 & & & 2\overline{\mu} & \\ & & & & & 2\overline{\mu} \end{pmatrix} \begin{pmatrix} \overline{\varepsilon}_{rr} \\ \overline{\varepsilon}_{\theta\theta} \\ \overline{\varepsilon}_{\phi\phi} \\ \overline{\varepsilon}_{r\theta} \\ \overline{\varepsilon}_{r\phi} \\ \overline{\varepsilon}_{\theta\phi} \end{pmatrix}. \tag{3.2}$$

Since the problem is spherically symmetric under the spherically symmetric displacement or the traction boundary condition, it is found that $\bar{\sigma}_{rr} \neq 0$, $\bar{\sigma}_{\theta\theta} = \bar{\sigma}_{\phi\phi} \neq 0$, $\bar{\sigma}_{r\theta} = \bar{\sigma}_{r\phi} = \bar{\sigma}_{\theta\phi} = 0$ and $\bar{\varepsilon}_{rr} \neq 0$, $\bar{\varepsilon}_{\theta\theta} = \bar{\varepsilon}_{\phi\phi} \neq 0$, $\bar{\varepsilon}_{r\theta} = \bar{\varepsilon}_{r\phi} = \bar{\varepsilon}_{\theta\phi} = 0$ so Eq. (3.2) is reduced to the following two independent algebraic equations:

$$\overline{\sigma}_{rr} = \left(\overline{K} + \frac{4}{3}\overline{\mu}\right)\overline{\varepsilon}_{rr} + \left(2\overline{K} - \frac{4}{3}\overline{\mu}\right)\overline{\varepsilon}_{\theta\theta}, \tag{3.3}$$

$$\overline{\sigma}_{\theta\theta} = \left(\overline{K} - \frac{2}{3}\overline{\mu}\right)\overline{\varepsilon}_{rr} + \left(\overline{K} + \frac{2}{3}\overline{\mu}\right)\overline{\varepsilon}_{\theta\theta}. \tag{3.4}$$

The solution to Eqs. (3.3) and (3.4) is found to provide the same upper and lower bounds of the effective bulk moduli with those of the energy approach in Eq. (3.1). However, it should be mentioned that the solution also contains the effective shear modulus, which is interesting to provide the same value of $\bar{\mu} = \mu_m$

when the spherically symmetric displacement or the traction boundary condition of Eq. (2.11) or (2.12) is applied. It is obvious that the upper and lower bounds of the effective shear modulus could not be simply μ_m but the same upper and lower bounds of the effective shear modulus correspond to the same upper and lower bounds of the effective bulk modulus.

Following the boundary approach in Section 2.5.3, the traction or displacement response on the outer surface of the composite sphere element can be found respectively under displacement or traction boundary condition, which is compared with that of a homogeneous equivalent medium to obtain the bounds of the effective bulk modulus. Since the problem is spherically symmetric, it is obvious that $t_r \neq 0$, $t_\theta = t_\phi = 0$ and $u_r \neq 0$, $u_\theta = u_\phi = 0$. Therefore, in the boundary approach to determine the effective bulk modulus, only one algebraic equation in the radial direction is involved, and the same upper and lower bounds of the effective bulk moduli are found with those of the energy approach in Eq. (3.1).

When the interface effect is considered, it can be seen from Eq. (3.1) that the effective bulk modulus depends on only one interface elastic constant, the interface bulk modulus Ks, as well as the size of nanoparticles.

If no interface effect is considered, Eq. (3.1) reduces to the classical solution [5] which is size-independent.

3.2. Effective shear modulus

When the transverse shear boundary condition of Eq. (2.13) or (2.14) is applied on the external surface of the matrix shell, the elastic field (displacement, strain and stress) in both the matrix and inhomogeneity has been found in Section 2.4.2. As mentioned in Section 2.5, for the transverse shear boundary condition, with the displacement field given with trigonometric functions in Eq. (2.16), the stress and strain field will also be trigonometric functions, so the volume integrals of the stress and strain field will be both zero and the effective shear modulus could not be determined by the average approach. Therefore, the effective shear modulus is obtained in the following by comparing the strain energy and the boundary response, respectively, of the composite sphere element with that of a homogeneous equivalent medium with the unknown effective elastic moduli under the same boundary conditions.

Following the energy approach in Section 2.5.1, the strain energy of the composite sphere element can be calculated by Eq. (2.25), which is compared with the strain energy of a homogeneous equivalent medium to obtain the bounds of the effective shear modulus. In contrast to the case of effective bulk modulus, the upper and lower bounds of the effective shear modulus are distinct as given below:

$$\overline{\mu}_{upper} = \frac{\overline{\mu}_{upper}^{numer}}{\overline{\mu}_{upper}^{denom}}, \qquad \overline{\mu}_{lower} = \frac{\overline{\mu}_{lower}^{numer}}{\overline{\mu}_{lower}^{denom}}, \tag{3.5}$$

where the expressions are too long to be listed in the main text and they are given in the Appendix.

Following the boundary approach in Section 2.5.3, the traction or displacement responses on the outer surface of the composite sphere element can be found, which is compared with that of a homogeneous equivalent medium to obtain the bounds of the effective shear modulus. When the transverse shear boundary condition of Eq. (2.13) or (2.14) is applied, with the displacement field given in Eq. (2.16), it is found that $t_r \neq 0$, $t_\theta = t_\phi \neq 0$ and $u_r \neq 0$, $u_\theta = u_\phi \neq 0$ Therefore, in the boundary approach to determine the effective shear modulus, two independent algebraic equations in the radial and circumferential directions should be satisfied simultaneously. However, it is found that the two independent equations conflict with each other when the transverse shear boundary condition is applied. This is due to the reason that the composite sphere element of Hashin's CSA model is not a neutral composite sphere [25] under the transverse shear boundary condition, i.e., if one inserts the composite sphere element in Fig. 1b back into the macroscopically isotropic composite medium in Fig. 1a, the originally uniform field of the composites outside the composite sphere region will be disturbed. On the contrary, the boundary approach works for the effective bulk modulus because the composite sphere element in Hashin's CSA model is a neutral composite sphere under the spherically symmetric boundary condition. Therefore, the effective bulk modulus could be obtained by the boundary approach but the effective shear modulus could not be obtained.

When the interface effect is considered, it can be seen from Eq. (3.5) that both upper and lower bounds of the effective shear modulus depend on two interface elastic constants, λ_s and μ_s, in a very complex way, which is in contrast to the simple case of the effective bulk modulus dependent on only the interface bulk modulus Ks. Furthermore, Eq. (3.5) shows that both upper and lower bounds of the effective shear modulus also depend on the size of nanoparticles.

When no interface effect is considered, Eq. (3.5) reduces to the size-indepenent classical solution in the following:

$$
\begin{aligned}
(3.6)_1 \quad & \overline{\mu}_{upper} = \\
& -500\mu_m\Big(-\Big(\Big(\nu_i+\frac{7}{5}\Big)\Big(\nu_m-\frac{7}{10}\Big)\mu_i-\mu_m\Big(\nu_i-\frac{7}{10}\Big)\Big(\nu_m-\frac{7}{5}\Big)\Big)(\mu_i-\mu_m)f^{\frac{10}{3}} \\
& +\Big(-2(\nu_i+\frac{7}{5})(\nu_m^2-\frac{3}{2}\nu_m+\frac{7}{8})\mu_i^2+\Big(\Big(\nu_i-\frac{14}{5}\Big)\nu_m^2 \\
& +\Big(\frac{33}{10}\nu_i+\frac{21}{10}\Big)\nu_m+\frac{49}{20}\nu_i-\frac{49}{20}\Big)\mu_m\mu_i+\mu_m^2\Big(\nu_i-\frac{7}{10}\Big)\Big(\nu_m^2-7\Big)\Big)f^{\frac{7}{3}} \\
& +\Big(\Big(\nu_i+\frac{7}{5}\Big)\mu_i-8\Big(\nu_i-\frac{7}{10}\Big)\mu_m\Big)\Big(\Big(\frac{63}{50}\mu_i-\frac{63}{50}\mu_m\Big)f^{\frac{5}{3}} \\
& +\Big((f+2)\nu_m^2-\Big(\frac{21}{10}f+3\Big)\nu_m+\frac{7}{20}f+\frac{28}{25}\Big)\mu_i
\end{aligned}
$$

$$
\begin{aligned}
&-\mu_m\Big((f-1)\nu_m^2+\Big(-\frac{21}{10}f+\frac{21}{10}\Big)\nu_m+\frac{7}{20}f-\frac{49}{50}\Big)\Big)\Big)\Big/\Big(-1000\Big(\Big(\nu_i+\frac{7}{5}\Big)\Big(\nu_m-\frac{7}{10}\Big)\mu_i\\
&-\mu_m\Big(\nu_i-\frac{7}{10}\Big)\Big(\nu_m+\frac{7}{5}\Big)\Big)(\mu_i-\mu_m)\Big(\nu_m*-\frac{4}{5}\Big)f^{\frac{10}{3}}+\Big(1000\Big(\nu_i+\frac{7}{5}\Big)\Big(\nu_m^2-\frac{3}{2}\nu_m+\frac{7}{8}\Big)\mu_i^2\\
&-500\Big(\Big(\nu_i-\frac{14}{5}\Big)\nu_m^2+\Big(\frac{33}{10}\nu_i+\frac{21}{10}\Big)\nu_m+\frac{49}{20}\nu_i-\frac{49}{20}\Big)\mu_m\mu_i-500\mu_m^2\Big(\nu_i-\frac{7}{10}\Big)(\nu_m^2-7)\Big)f^{\frac{7}{3}}\\
&+1000\Big(\nu_i+\frac{7}{5}\Big)\mu_i-8\Big(\nu_i-\frac{7}{10}\Big)\mu_m\Big)\Big(\Big(-\frac{63}{100}\mu_i+\frac{63}{100}\mu_m\Big)f^{\frac{5}{3}}\\
&+\Big((f-1)\nu_m^2-\Big(\frac{3}{2}f+\frac{21}{20}\Big)\nu_m+\frac{7}{8}f-\frac{14}{25}\Big)\mu_i\\
&-\mu_m\Big(\Big(f+\frac{1}{2}\Big)\nu_m^2+\Big(-\frac{3}{2}f-\frac{21}{20}\Big)\nu_m+\frac{7}{8}f+\frac{49}{100}\Big)\Big)\Big),
\end{aligned}
$$

$(3.6)_2$ $\quad \overline{\mu}_{lower} =$

$$
\begin{aligned}
&-125\mu_m(-8(\mu_i-\mu_m)\Big(\nu_m-\frac{7}{5}\Big)\Big(\Big(\nu_i+\frac{7}{5}\Big)\Big(\nu_m-\frac{7}{10}\Big)\mu_i-\mu_m\Big(\nu_m+\frac{7}{5}\Big)\Big(\nu_i-\frac{7}{10}\Big)\Big)f^{\frac{10}{3}}\\
&+\Big(-16\Big(\nu_m^2-\frac{3}{2}\nu_m+\frac{7}{8}\Big)\Big(\nu_i+\frac{7}{5}\Big)\mu_i^2+8\mu_m\Big(\Big(\nu_i-\frac{14}{5}\Big)\nu_m^2+\Big(\frac{33}{10}\nu_i+\frac{21}{10}\Big)\nu_m+\frac{49}{20}\nu_i-\frac{49}{20}\Big)\mu_i\\
&+8\mu_m^2\Big(\nu_i-\frac{7}{10}\Big)(\nu_m^2-7)\Big)f^{\frac{7}{3}}+\Big(\Big(\nu_i+\frac{7}{5}\Big)\mu_i-8\Big(\nu_i-\frac{7}{10}\Big)\mu_m\Big)\Big(\Big(\frac{252}{25}(\mu_i-\mu_m)f^{\frac{5}{3}}\\
&+\Big((f+2)\nu_m^2+\frac{6}{5}\nu_m-7f-\frac{56}{25}\Big)\mu_i-\mu_m\Big((f-1)\nu_m^2-7f+\frac{49}{25}\Big)\Big/\\
&\Big(-2000(\mu_i-\mu_m)\Big(\Big(\nu_i+\frac{7}{5}\Big)\Big(\nu_m-\frac{7}{10}\Big)\mu_i-\mu_m\Big(\nu_m+\frac{7}{5}\Big)\Big(\nu_i-\frac{7}{10}\Big)\Big)\Big(\nu_m-\frac{4}{5}\Big)f^{\frac{10}{3}}\\
&+\Big(2000\Big(\nu_m^2-\frac{3}{2}\nu_m+\frac{7}{8}\Big)\Big(\nu_i+\frac{7}{5}\Big)\mu_i^2-1000\mu_m\Big(\Big(\nu_i-\frac{14}{5}\Big)\nu_m^2+\Big(\frac{33}{10}\nu_i+\frac{21}{10}\Big)\nu_m\\
&+\frac{49}{20}(\nu_i-1)\Big)\mu_i-1000\mu_m^2\Big(\nu_i-\frac{7}{10}\Big)(\nu_m^2-7)\Big)f^{\frac{7}{3}}+250\Big(\Big(-\frac{126}{25}\mu_i+\frac{126}{25}\Big)f^{\frac{5}{3}}\\
&+\Big((f-1)\nu_m^2+\frac{3}{5}(f-1)\nu_m+\frac{7}{5}f+\frac{28}{25}\Big)\mu_i\\
&-\Big(\Big(f+\frac{1}{2}\Big)\nu_m^2+\frac{3}{5}f\nu_m+\frac{7}{5}f-\frac{49}{50}\Big)\mu_m\Big)\Big(\Big(\nu_i+\frac{7}{5}\Big)\mu_i-8\mu_m\Big(\nu_i-\frac{7}{10}\Big)\Big)\Big).
\end{aligned}
$$

The result in Eq. (3.6) is provided as an explicit closed-form solution, which is checked to be consistent with the implicit classical solution [5]. Moreover, if the volume fraction of particles is very small, the upper and lower bounds of the effective shear modulus in Eq. (3.6) are approximated as:

$$
\overline{\mu}_{upper} = \overline{\mu}_{lower} = \mu_m\Big(1-\frac{15(1-\nu_m)\big(1-\frac{\mu_i}{\mu_m}\big)}{7-5\nu_m+2(4-5\nu_m)\frac{\mu_i}{\mu_m}}f\Big), \tag{3.7}
$$

which indicates that both bounds coincide and reduce to the shear modulus of the matrix as expected when the particle concentration is close to zero ($f \to 0$).

Similarly, if the volume fraction of particles is very large ($f \to 1$), the upper and lower bounds of the effective shear modulus in Eq. (3.6) are approximated as:

$$(3.8)\quad \overline{\mu}_{upper} = \overline{\mu}_{lower} = \mu_i\left(1 - \frac{(1-\frac{\mu_m}{\mu_i})\left(7-5\nu_m+2(4-5\nu_m)\frac{\mu_i}{\mu_m}\right)}{15(1-\nu_m)}(1-f)\right),$$

which indicates that both bounds coincide and reduce to the shear modulus of the particle as expected when the particle concentration is close to 1 ($f \to 1$).

3.3. Comparison with experiment results

With the closed-form solution to the upper and lower bounds of the effective elastic moduli of nanoparticle-reinforced composites, the theoretical result can be used for numerical comparisons with experimental results. In the following, the experimental result [44] of the elastic moduli of rubber-toughened poly (methylmethacrylate) (RT-PMMA) with different rubber particle fractions is used for comparison. Transmission electron microscopy on the specimens reveals that the rubber particles have nearly spherical shapes with the diameter ranging from 50 nm to 100 nm, which could be fairly approximated by the theoretical solution with the average radius of the rubber particles set to $a = 37.5$ nm. In the experimental report, the elastic moduli of the rubber reinforcement and PMMA matrix are given as: $K_i = 2.60$ GPa, $\mu_i = 0.54$ GPa, $\nu_i = 0.40$ and $K_m = 5.91$ GPa, $\mu_m = 2.25$ GPa, $\nu_m = 0.33$, respectively. To consider the interface effect, the interface elastic constants of the rubber/PMMA interface should be provided. Unfortunately, the interface elastic property of solids is extremely difficult to obtain by experiments, and the only related experimental result is the recent report [45, 46] on the surface elastic constants of a soft polymer gel through microscopic observations of the contact-line geometry of a partially wetting droplet on an anisotropically stretched substrate. However, atomistic simulations indicate that surface/interface elastic constants are between -10 N/m and 10 N/m for many metallic crystals and semiconductors [47–52]. Unlike the positive definiteness of the bulk stiffness tensor to guarantee the stability of the material, the surface/interface stiffness tensor does not need to be positive definite because the surface/interface cannot exist independent of the bulk material, so the stability of the material is maintained as long as the total energy (bulk+surface/interface) satisfies the positive definiteness condition. In our calculation, the interface elastic constants are set to $\lambda_s = 5$ N/ m, $\mu_s = -2.5$ N/m with $K_s = 2.5$ N/m as an illustration of the interface effect.

Figure 2 shows the theoretical and experimental results of the effective moduli of RT-PMMA composites for different rubber volume fractions with and without the consideration of the interface effect. Both the effective bulk modulus (Fig. 2a) and effective shear modulus (Fig. 2b) of the composites decrease when the rubber volume fraction increases because the elastic moduli of rubber particles are smaller than those of the PMMA matrix. For comparisons, the

Hashin–Shtrikman bound solutions [7] and exact solutions by GSCM [24] are added together.

For the effective bulk modulus of composites, the Hashin–Shtrikman upper and lower bounds are distinct while those by Hashin's CSA model in Eq. (3.1) are the same and coincide with the exact solution by GSCM, so the bound solution in Eq. (3.1) and the exact solution by GSCM of the effective bulk modulus is just

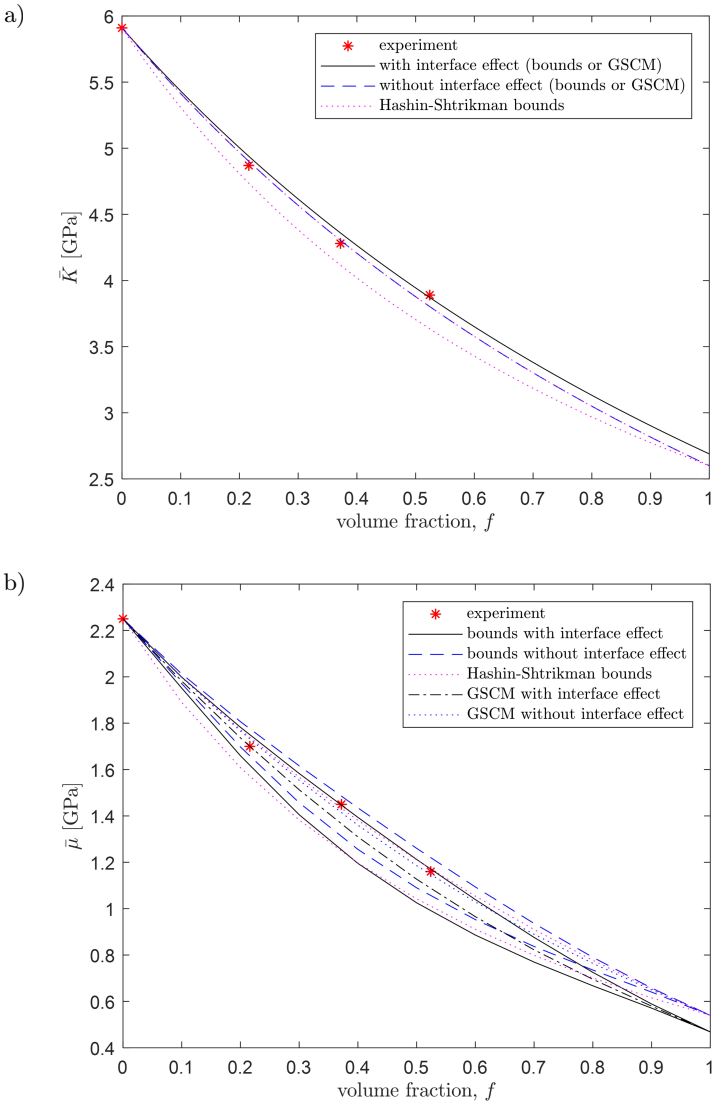

FIG. 2. Effective moduli of RT-PMMA composites with different rubber volume fractions; a) bulk modulus, b) shear modulus.

a single curve with or without the interface effect respectively. In Fig. 2a, when the interface effect is not considered, the exact solution by GSCM and bounds by Hashin's CSA model are essentially identical to the Hashin–Shtrikman upper bound as expected from their formulae. Furthermore, it should be noticed that the solutions with or without the interface effect are distinct at the limit of $f = 1$, which is discussed in detail in Section 4.3.

On the other hand, for the effective shear modulus of composites, the upper and lower bounds of all the bound solutions are distinct so there are two curves for each bound solution with or without the consideration of the interface effect. In Fig. 2b, when the interface effect is not considered, the Hashin-Shtrikman bounds are different from those by Hashin's CSA model in Eq. (3.6) because the Hashin–Shtrikman bounds are irrespective of the microstructural arrangement of the composite in contrast to the arrangement requirement of Hashin's CSA model as illustrated in Section 2.1. Moreover, the exact solutions by GSCM are validated as setting well between the bound solutions with or without the consideration of the interface effect respectively. Similar to the effective bulk modulus in Fig. 2a, the solutions to the effective shear modulus with or without the interface effect are distinct at the limit of $f = 1$, which is discussed in detail in Section 4.3.

Furthermore, it can be seen that the theoretical results with and without the consideration of the interface effect are not different significantly, although both agree well with the experimental results of the effective moduli of RT-PMMA composites for different rubber volume fractions. Therefore, for such specific composites, the interface effect is not necessarily important because the particle size is still fairly large to demonstrate the interface effect. Unfortunately, experimental results of the elastic moduli of nanoparticle-reinforced composites are very rare, and the particle size in experiments are usually several microns or above. This might be the reason that only theoretical results of the elastic moduli of nanoparticle-reinforced composites with the interface effect are reported as far as the authors have found in the literature. However, the bounds of the effective moduli of nanoparticle-reinforced composites are indeed found to depend on the interface elastic constants and the size of nanoparticles, which is discussed in detail in the following.

4. Discussions

In Section 3, based on the CSA and the interface stress model, the upper and lower bounds of the effective bulk modulus of nanoparticle-reinforced composites are found to coincide in Eq. (3.1) by three different approaches, while distinct upper and lower bounds of the effective shear modulus are found in Eq. (3.5) by the energy approach. For nanomaterials, both Eq. (3.1) and Eq. (3.5) indicate

that the effective elastic moduli of nanoparticle-reinforced composites depend on the interface elastic constants and the size of nanoparticles, which are important for the fabrication and design of nanomaterials.

4.1. Interface effect

Figure 3 shows the change of the effective bulk modulus with different volume fractions of nanoparticles for different interface elastic constants. The elastic moduli of the nanoparticles and matrix are the same with those in Section 3.3, and the size of nanoparticles is set to 50 nm. Since interface elastic constants are usually between $-10\,\mathrm{N/m}$ and $10\,\mathrm{N/m}$ for solids, the interface bulk modulus is set to $0, \pm 5, \pm 10\,\mathrm{N/m}$ respectively. The case of $K_s = 0\,\mathrm{N/m}$ corresponds to the classical solution which takes no interface effect into consideration. It is obviously seen that the result of the effective bulk modulus with a different interface bulk modulus is distinct compared with the classical solution. The difference between the classical solution and all the other curves with the consideration of the interface effect become more significant when the volume fraction of nanoparticles increases, which is as expected because the total interface-to-volume ratio increases with more nanoparticles. When the interface bulk modulus is positive, the effective bulk modulus is larger than the classical solution and vice versa. The larger the interface bulk modulus is, the more effective bulk modulus deviates from the classical solution. When the interface bulk modulus is extremely

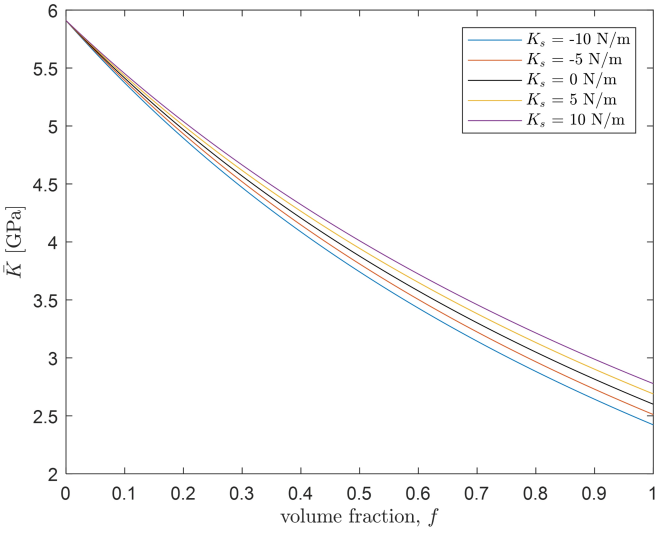

FIG. 3. Change of the effective bulk modulus with different volume fractions of nanoparticles for different interface elastic constants.

small, the curves tend to converge to the classical solution. This monotonically increasing behavior could be easily proven as the derivative of the effective bulk modulus in Eq. (3.1) with respect to the interface bulk modulus is strictly positive thanks to the closed-form solution:

$$\frac{d\bar{K}}{dK_s} = \frac{4af}{27}\left(\frac{3K_m + 4\mu_m}{\left(f(K_i - K_m) - K_i - \frac{4}{3}\mu_m\right)a - \frac{4}{3}K_s(1-f)}\right)^2 > 0. \tag{4.1}$$

Figure 4 shows the change of the effective shear modulus with different volume fractions of nanoparticles for different interface elastic constants. The elastic moduli of the nanoparticles and matrix are the same with those in Section 3.3, and the size of nanoparticles is set to 50 nm. Similar to the effective bulk modulus, the difference between the classical solution and all the other curves for the effective shear modulus with the consideration of the interface effect become more significant when the volume fraction of nanoparticles increases. In Fig. 4, to consider the interface effect, the interface elastic constant λ_s is fixed to 2.5 N/m, while the other interface elastic constant μ_s is set to ± 1.5 N/m for comparison. In this case, both the upper and lower bounds of the effective shear modulus are larger than those of the classical solution with $\mu_s = 1.5$ N/m, but they are smaller than those of the classical solution with $\mu_s = -1.5$ N/m. It should be noted that the effective shear modulus depends on two interface elastic constants, λ_S and μ_S, in contrast to the case that the effective bulk modulus only depends on the interface bulk modulus K_s. Therefore, unlike the monotonically

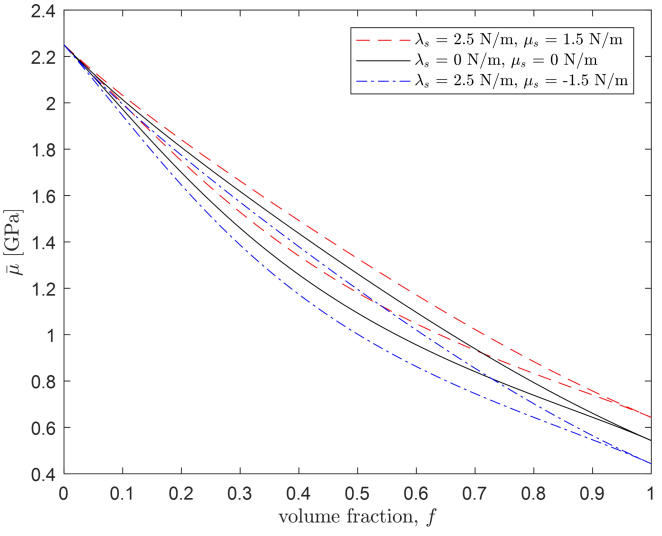

FIG. 4. Change of the effective shear modulus with different volume fractions of nanoparticles for different interface elastic constants.

increasing behavior of the effective bulk modulus with respect to the interface bulk modulus, the changing trend of the effective shear modulus with respect to the two interface elastic constants is much more complex as can be seen from the complicated analytical expressions in the Appendix. Furthermore, there is in fact a tiny numeric difference between the bounds of the effective shear modulus by consideration of the interface effect at the limit of $f = 1$ which is difficult to notice for the red dashed and blue dash-dotted curves in Fig. 4. This unexpected limiting behavior of the bounds of the effective shear modulus is discussed in detail in Section 4.3.

4.2. Size effect

Figure 5 shows the change of the effective bulk modulus with different volume fractions of nanoparticles for different sizes of nanoparticles. The elastic moduli of the nanoparticles and matrix are the same with those in Section 3.3, and the interface bulk modulus is fixed to $K_s = 10\,\mathrm{N/m}$. On the other hand, Fig. 6 shows the change of the effective shear modulus with different volume fractions of nanoparticles for different sizes of nanoparticles. The elastic moduli of the nanoparticles and matrix are the same with those in Section 3.3, and the interface elastic constants are fixed to $\lambda_s = 10\,\mathrm{N/m}$, $\mu_s = -5\,\mathrm{N/m}$. In Figs. 5 and 6, It is obviously seen that the results of the effective bulk and shear moduli with different sizes of nanoparticles are different, which is a typical size-dependent

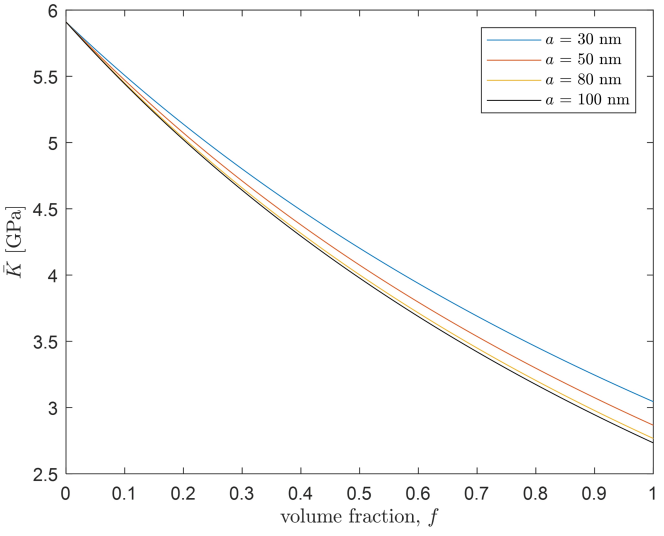

FIG. 5. Change of the effective bulk modulus with different volume fractions of nanoparticles for different sizes of nanoparticles.

behavior of nanomaterials. Moreover, if the size of nanoparticles reaches above 100 nm, both the effective bulk and shear moduli tend to converge to the classical solution. This is as expected because the interface effect only plays an important role at nano scales in determining the behavior of nanoparticle-reinforced composites. However, in Figs. 5 and 6, when the size of nanoparticles increases, the effective bulk modulus decreases while both the upper and lower bounds of the effective shear modulus increase on the contrary.

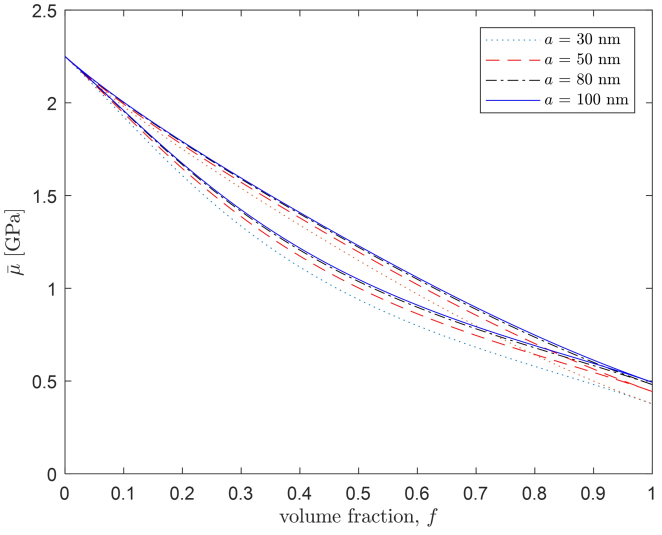

FIG. 6. Change of the effective shear modulus with different volume fractions of nanoparticles for different sizes of nanoparticles.

4.3. Limit analysis

For the classical case without the interface effect, when the particle concentration takes the limit of 0 or 1, it is obvious that the bounds of the effective elastic moduli of conventional composites should coincide and converge to those of the matrix and particle, respectively. In the following, limit analysis is performed on the bounds of the effective elastic moduli of nanoparticle-reinforced composites when the particle concentration is extremely small or large. Some unexpected results are found which may be unnoted in the literature.

Firstly, by setting $f = 0$ in Eq. (3.1), i.e., when the nanocomposites become pure matrix, the bounds of the effective bulk modulus coincide and converge to the bulk modulus of the matrix similar to the classical case. However, by setting $f = 1$ in Eq. (3.1), i.e., when the nanocomposites become pure nanoparticles,

the bounds again coincide but converge to:

$$\overline{K}_{upper}|_{f=1} = \overline{K}_{lower}|_{f=1} = K_i + \Delta K = K_i + \frac{4K_s}{3a}, \tag{4.2}$$

where $\Delta K = 4K_s/3a$ is the difference from the bulk modulus of particle (K_i) in the classical case. In essence, the parameter K_s in Eq. (4.2) should be interpreted as surface bulk modulus instead of interface bulk modulus. It is identical to Eq. (54) (neglecting the third-order bulk elastic constants) of DINGREVILLE *et al.* [22] for the exact solution to the effective stiffness tensor of spherical nanoparticles. Furthermore, since $K_i \sim$ GPa and $K_s \sim$ N/m, the difference ΔK is comparable to the bulk modulus K_i, i.e., $\Delta K \sim K_i$ when the particle shrinks to nanoparticles ($a \sim$ nm).

Secondly, by setting $f = 0$ in Eq. (3.5), the bounds of the effective shear modulus coincide and converge to the shear modulus of the matrix similar to the classical case. However, by setting $f = 1$ in Eq. (3.5), the bounds of the effective shear modulus of pure spherical nanoparticles become distinct. Specifically, the upper bound is reduced to:

$$\overline{\mu}_{upper}|_{f=1} = \mu_i + \Delta\mu = \mu_i + \frac{7\mu_s + \lambda_s}{5a}, \tag{4.3}$$

where $\Delta\mu = (7\mu_s + \lambda_s)/5a$ is the difference from the shear modulus of particle (μ_i) in the classical case and it is comparable to the shear modulus μ_i, i.e., $\Delta\mu \sim \mu_i$ for nanoparticles as $\mu_i \sim$ GPa and $\mu_s, \lambda_s \sim$ N/m. Equation (4.3) is also identical to Eq. (55) (neglecting the third-order bulk elastic constants) of DINGREVILLE *et al.* [22] for the exact solution to the effective stiffness tensor of spherical nanoparticles.

On the contrary, the lower bound of the effective shear modulus of pure nanoparticles is distinct and reduced to:

$$\overline{\mu}_{lower}|_{f=1} = \overline{\mu}_{upper}|_{f=1} + \Delta\overline{\mu} = \mu_i + \Delta\mu + \Delta\overline{\mu}, \tag{4.4}$$

where $\Delta\bar{\mu}$ denotes the difference from the upper bound of the effective shear modulus of pure nanoparticles:

$$\Delta\overline{\mu} = -\frac{24}{\mu_i \frac{5\nu_i+7}{7-10\nu_i} + \frac{4(7\mu_s+6\lambda_s)}{5a}} \left(\frac{2\mu_s + \lambda_s}{5a}\right)^2. \tag{4.5}$$

It is seen in Eq. (4.5) that $\Delta\bar{\mu} \sim$ GPa for nanoparticles as $\mu_i \sim$ GPa and $\mu_s, \lambda_s \sim$ N/m, so $\Delta\bar{\mu}$ is also comparable to the shear modulus μ_i similar to $\Delta\mu \sim \mu_i$ for nanoparticles. However, this difference between the bounds of the effective shear modulus of pure nanoparticles is not seen in Fig. 2b or Fig. 6 at

the limit of $f = 1$ because the interface elastic constants happen to be set to $2\mu_s + \lambda_s = 0$ that leads to $\Delta\bar{\mu} = 0$ according to Eq. (4.5). As mentioned earlier, there is in fact a tiny numeric difference between the bounds of the effective shear modulus with the interface effect at the limit of $f = 1$ which is difficult to notice for the red dashed and blue dash-dotted curves in Fig. 4 because the particle size is fairly large ($a = 50\,\text{nm}$). To illustrate the difference $\Delta\bar{\mu}$ between the bounds of the effective shear modulus with the interface effect, the particle size is shrunk to $a = 5\,\text{nm}$ and Fig. 4 is redrawn as Fig. 7 below. It is very obvious from the red dashed curve in Fig. 7 to see the difference between the bounds of the effective shear modulus of pure nanoparticles at the limit of $f = 1$ for interface elastic constants $\lambda_s = 2.5\,\text{Nm}$, $\mu_s = 1.5\,\text{N/m}$, while the difference is still unnoticeable from the blue dash-dotted curve in Fig. 7 for the case of interface elastic constants $\lambda_s = 2.5\,\text{N/m}$, $\mu_s = -1.5\,\text{N/m}$ as $\Delta\bar{\mu}$ is still very small according to Eq. (4.5).

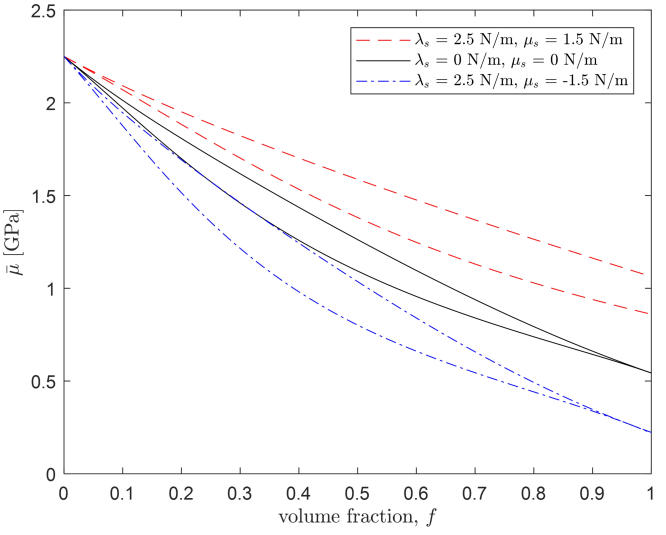

FIG. 7. Change of the effective shear modulus with different volume fractions of nanoparticles ($a = 5\,\text{nm}$).

It is unexpected to see that the bounds of the effective shear modulus of pure nanoparticles deviate from each other in contrast to the effective bulk modulus of nanoparticles or both effective moduli of conventional composites. This could be explained by invoking the interface stress model and the concept of neutral inclusion. In the classical case of conventional composites under the transverse shear boundary condition, the non-neutral composite sphere element becomes a neutral particle as no matrix is involved, thus the bounds of the effective shear

modulus of conventional composites coincide at the limit of $f = 1$. On the contrary, in the case of nanocomposites, from the interface stress model of Eqs. (2.7) and (2.8), the stress jump in nanoparticles across the interface (or surface exactly) can be regarded to be from the nanoparticle to void as an imaginary matrix, so the non-neutral composite sphere element in nanocomposites is still non-neutral as a nanoparticle that leads to distinct bounds of the effective shear modulus of pure nanoparticles. As for the effective bulk modulus, the composite sphere element is a neutral composite sphere regardless of the existence of the interface effect under the spherically symmetric boundary condition, so the bounds of the effective bulk modulus of conventional composites or nanocomposites always coincide.

5. Conclusions

This work investigates the bounds of the effective elastic moduli of nanoparticle-reinforced composites based on the CSA and interface stress models. The elastic field is solved as the boundary value problem in the theory of elasticity based on the CSA and interface stress models, which is then used to derive the bounds of the effective elastic moduli. Three different approaches are formulated by comparing the strain energy, average stress and strain, and boundary responses, respectively, of the composite sphere element with that of a homogeneous equivalent medium under the same boundary conditions. It is found that the effective bulk modulus can be obtained by all three different approaches but the effective shear modulus can be obtained only by the energy approach. The bounds of the effective bulk modulus coincide and depend only on the interface bulk modulus, while those of the effective shear modulus are distinct and depend on two interface elastic constants. The influences of the interface effect and the size of nanoparticles on the bounds of the effective elastic moduli of nanoparticle-reinforced composites are discussed in detail, which are important for the fabrication and design of nanomaterials. Moreover, the limit analysis discloses that the bounds of the effective bulk modulus of pure spherical nanoparticles coincide but deviate from the bulk modulus of particle in the classical case, and the bounds of the effective shear modulus are distinct in contrast to the effective bulk modulus of pure spherical nanoparticles or both effective moduli of conventional composites.

Declarations

The authors have no conflicts of interest to declare that are relevant to the content of this article.

Appendix

Using softwares like Maple or Mathematica, the expressions are given as:

$$
\begin{aligned}
&\overline{\mu}_{upper}^{numer} = \\
&1000\mu_m\Big(\frac{1}{2}\Big(\nu_m-\frac{7}{5}\Big)\Big(\Big(\Big((\mu_i-\mu_m)\nu_i+\frac{7}{5}\mu_i+\frac{7}{10}\mu_m\Big)\nu_m \\
&+\Big(-\frac{7}{10}\mu_i-\frac{7}{5}\mu_m\Big)\nu_i-\frac{49}{50}\mu_i+\frac{49}{50}\mu_m\Big)(\mu_i-\mu_m)a^2+\Big(\Big(-\frac{49}{5}(\mu_s+\frac{47}{49}\lambda_s)(\mu_i-\mu_m)\nu_i \\
&+\Big(\frac{49}{5}\mu_s+7\lambda_s\Big)\mu_i-\frac{343}{50}\Big(\mu_s+\frac{47}{49}\lambda_s\Big)\mu_m\Big)\nu_m+\Big(\Big(\frac{329}{50}\lambda_s+\frac{343}{50}\mu_s\Big)\mu_i-\frac{49}{5}\Big(\mu_s+\frac{5}{7}\lambda_s\Big)\mu_m\Big)\nu_i \\
&-\frac{343}{50}\Big(\mu_s+\frac{5}{7}\lambda_s\Big)(\mu_i-\mu_m)a-8\Big(\nu_i-\frac{7}{10}\Big)\mu_s\Big(\nu_m-\frac{7}{10}\Big)(\mu_s+\lambda_s)f^{\frac{10}{3}} \\
&+(\Big(\Big((\mu_i-\mu_m)\nu_i+\frac{7}{5}\mu_i+\frac{7}{10}\mu_m\Big)\Big(\mu_i+\frac{1}{2}\mu_m\Big)\nu_m^2-\frac{3}{2}\mu_i\Big(\Big(\mu_i+\frac{11}{10}\mu_m\Big)\nu_i+\frac{7}{5}\mu_i+\frac{7}{10}\mu_m\Big)\nu_m \\
&+\Big(\frac{7}{8}\mu_i^2-\frac{49}{40}\mu_i\mu_m+\frac{7}{2}\mu_m^2\Big)\nu_i+\frac{49}{40}(\mu_i+2\mu_m)(\mu_i-\mu_m)\Big)a^2 \\
&+\Big(\Big(\Big(\Big(-\frac{49}{5}\mu_s-\frac{47}{5}\lambda_s\Big)\mu_i-7(\mu_s+\frac{5}{7}\lambda_s)\mu_m\Big)\nu_i+\frac{49}{5}\Big(\mu_s+\frac{5}{7}\lambda_s\Big)\Big(\mu_i+\frac{1}{2}\mu_m\Big)\Big)\nu_m^2 \\
&+\Big(\Big(\Big(\frac{147}{10}\mu_s+\frac{141}{10}\lambda_s\Big)\mu_i+21(\mu_s+\frac{5}{7}\lambda_s)\mu_m\Big)\nu_i-\frac{147}{10}(\mu_s+\frac{5}{7}\lambda_s)(\mu_i+\mu_m)\Big)\nu_m \\
&+\Big(\Big(-\frac{343}{40}\mu_s-\frac{329}{40}\lambda_s\Big)\mu_i-14\mu_m\Big(\mu_s+\frac{1}{2}\lambda_s\Big)\Big)\nu_i+\Big(\frac{343}{40}\mu_s+\frac{49}{8}\lambda_s\Big)\mu_i+\frac{49}{5}\mu_m\Big(\mu_s+\frac{1}{2}\lambda_s\Big)\Big)a \\
&-8\mu_s\Big(\nu_m^2-\frac{3}{2}\nu_m+\frac{7}{8}\Big)\Big(\nu_i-\frac{7}{10}\Big)(\mu_s+\lambda_s)f^{\frac{7}{3}}+\Big(-\frac{63}{100}(\mu_i-\mu_m)\Big((\mu_i-8\mu_m)\nu_i+\frac{7}{5}\mu_i+\frac{28}{5}\mu_m\Big)a^2 \\
&+\Big(-\frac{252}{25}\Big(\nu_i-\frac{7}{10}\Big)\mu_m\Big(\mu_s+\frac{1}{2}\lambda_s\Big)\nu_m+\Big(\Big(\frac{3087}{500}\mu_s+\frac{2961}{500}\lambda_s\Big)\mu_i+\frac{252}{25}\mu_m\mu_s\Big)\nu_i \\
&+\Big(-\frac{3087}{500}\mu_s-\frac{441}{100}\lambda_s\Big)\mu_i-\frac{882}{125}\mu_m\mu_s\Big)a+\frac{126}{25}\mu_s\Big(\nu_i-\frac{7}{10}\Big)(\mu_s+\lambda_s)f^{\frac{5}{3}} \\
&-\frac{1}{2}\Big(((f+2)\mu_i-\mu_m(f-1))\nu_m^2+\Big(\Big(-\frac{21}{10}f-3\Big)\mu_i+\frac{21}{10}\mu_m(f-1)\Big)\nu_m \\
&+\Big(\frac{7}{20}f+\frac{28}{25}\Big)\mu_i-\frac{7}{20}\mu_m\Big(f-\frac{14}{5}\Big)\Big)\Big((\mu_i-8\mu_m)\nu_i+\frac{7}{5}\mu_i+\frac{28}{5}\mu_m\Big)a^2 \\
&+\Big(\Big(\Big(\frac{49}{10}\Big(\mu_s+\frac{47}{49}\lambda_s\Big)(f+2)\mu_i-4\mu_m\Big(-\frac{21}{5}\mu_s+\lambda_s\Big(f-\frac{8}{5}\Big)\Big)\Big)\nu_i \\
&-\frac{49}{10}\Big(\mu_s+\frac{5}{7}\lambda_s\Big)(f+2)\mu_i+\frac{14}{5}\mu_m\Big(-\frac{21}{5}\mu_s+\lambda_s\Big(f-\frac{8}{5}\Big)\Big)\Big)\nu_m^2 \\
&+\Big(\Big(-\frac{1029}{100}(\mu_s+\frac{47}{49}\lambda_s)(f+\frac{7}{10})\mu_i+\frac{42}{5}\Big(-\frac{17}{5}\mu_s+\lambda_s\Big(f-\frac{52}{35}\Big)\Big)\mu_m\Big)\nu_i \\
&+\frac{1029}{100}\Big(f+\frac{10}{7}\Big)\Big(\mu_s+\frac{5}{7}\lambda_s\Big)\mu_i-\frac{147}{25}\Big(-\frac{17}{5}\mu_s+\lambda_s\Big(f-\frac{52}{35}\Big)\Big)\mu_m\Big)\nu_m \\
&+\Big(\frac{343}{200}\Big(\mu_s+\frac{47}{49}\lambda_s\Big)\Big(f+\frac{16}{5}\Big)\mu_i-\frac{7}{5}\Big(-\frac{42}{5}\mu_s+\lambda_s(f-4)\Big)\mu_m\Big)\nu_i
\end{aligned}
$$

$$-\frac{343}{200}\left(\mu_s+\frac{5}{7}\lambda_s\right)\left(f+\frac{16}{5}\right)\mu_i+\frac{49}{50}\left(-\frac{42}{5}\mu_s+\lambda_s(f-4)\right)\mu_m\Big)a$$
$$+4\left(\nu_i-\frac{7}{10}\right)\left((f+2)\nu_m^2+\left(-\frac{21}{10}f-3\right)\nu_m+\frac{7}{20}f+\frac{28}{25}\right)\mu_s(\mu_s+\lambda_s)\Big),$$

$$\overline{\mu}_{upper}^{denom}=$$
$$-1000\Bigg(\Bigg(\Bigg((\mu_i-\mu_m)\nu_i+\frac{7}{5}\mu_i+\frac{7}{10}\mu_m\Bigg)\nu_m+\left(-\frac{7}{10}\mu_i-\frac{7}{5}\mu_m\right)\nu_i-\frac{49}{50}\mu_i+\frac{49}{50}\mu_m\Bigg)(\mu_i-\mu_m)a^2$$
$$+\Bigg(\left(-\frac{49}{5}\left(\mu_s+\frac{47}{49}\lambda_s\right)(\mu_i-\mu_m)\nu_i+\left(\frac{49}{5}\mu_s+7\lambda_s\right)\mu_i-\frac{343}{50}\left(\mu_s+\frac{47}{49}\lambda_s\right)\mu_m\right)\nu_m$$
$$+\left(\left(\frac{329}{50}\lambda_s+\frac{343}{50}\mu_s\right)\mu_i-\frac{49}{5}\left(\mu_s+\frac{5}{7}\lambda_s\right)\mu_m\right)\nu_i-\frac{343}{50}\left(\mu_s+\frac{5}{7}\lambda_s\right)(\mu_i-\mu_m)a$$
$$-8\left(\nu_i-\frac{7}{10}\right)\mu_s\left(\nu_m-\frac{7}{10}\right)(\mu_s+\lambda_s)\left(\nu_m-\frac{4}{5}\right)f^{\frac{10}{3}}+\Bigg(\Bigg(1000\Bigg((\mu_i-\mu_m)\nu_i+\frac{7}{5}\mu_i+\frac{7}{10}\mu_m\Bigg)$$
$$\times\left(\mu_i+\frac{1}{2}\mu_m\right)\nu_m^2-1500\mu_i\Bigg(\left(\mu_i+\frac{11}{10}\mu_m\right)\nu_i+\frac{7}{5}\mu_i+\frac{7}{10}\mu_m\Bigg)\nu_m+(875\mu_i^2-1225\mu_i\mu_m+3500\mu_m^2)\nu_i$$
$$+1225(\mu_i+2\mu_m)(\mu_i-\mu_m)\Bigg)a^2+\Bigg(\Bigg(\Bigg((-9800\mu_s-9400\lambda_s)\mu_i-7000\left(\mu_s+\frac{5}{7}\lambda_s\right)\mu_m\Bigg)\nu_i$$
$$+9800\left(\mu_s+\frac{5}{7}\lambda_s\right)\left(\mu_i+\frac{1}{2}\mu_m\right)\Bigg)\nu_m^2+\Bigg(\Bigg(\left(14700\mu_s+14100\lambda_s\right)\mu_i+21000\left(\mu_s+\frac{5}{7}\lambda_s\right)\mu_m\Bigg)\nu_i$$
$$-14700\left(\mu_s+\frac{5}{7}\lambda_s\right)(\mu_i+\mu_m)\Bigg)\nu_m+\Bigg(\left(-8575\mu_s-8225\lambda_s\right)\mu_i-14000\mu_m\left(\mu_s+\frac{1}{2}\lambda_s\right)\Bigg)\nu_i$$
$$+(8575\mu_s+6125\lambda_s)\mu_i+9800\mu_m\left(\mu_s+\frac{1}{2}\lambda_s\right)\Bigg)a-8000\mu_s\left(\nu_m^2-\frac{3}{2}\nu_m+\frac{7}{8}\right)\left(\nu_i-\frac{7}{10}\right)(\mu_s+\lambda_s)f^{\frac{7}{3}}$$
$$+\Bigg(-630(\mu_i-\mu_m)\left((\mu_i-8\mu_m)\nu_i+\frac{7}{5}\mu_i+\frac{28}{5}\mu_m\right)a^2+\Bigg(-10080\left(\nu_i-\frac{7}{10}\right)\mu_m\left(\mu_s+\frac{1}{2}\lambda_s\right)\nu_m$$
$$+((6174\mu_s+5922\lambda_s)\mu_i+10080\mu_m\mu_s)\nu_i+(-6174\mu_s-4410\lambda_s)\mu_i-7056\mu_m\mu_s)a$$
$$+5040\mu_s\left(\nu_i-\frac{7}{10}\right)(\mu_s+\lambda_s)f^{\frac{5}{3}}+1000\Bigg(\Bigg((f-1)\mu_i-\left(f+\frac{1}{2}\right)\mu_m\Bigg)\nu_m^2$$
$$+\Bigg(\left(-\frac{3}{2}f+\frac{3}{2}\right)\mu_i+\frac{3}{2}\left(f+\frac{7}{10}\right)\mu_m\Bigg)\nu_m+\left(\frac{7}{8}\left(f+\frac{14}{25}\right)\mu_m\left((\mu_i-8\mu_m)\nu_i+\frac{7}{5}\mu_i+\frac{28}{5}\mu_m\right)a^2$$
$$+\Bigg(\Bigg(\Bigg(-9800\left(\mu_s+\frac{47}{49}\lambda_s\right)(f-1)\mu_i+8000\mu_m\left(\frac{21}{10}\mu_s+\lambda_s\left(f+\frac{4}{5}\right)\right)\Bigg)\Bigg)\nu_i$$
$$+9800\left(\mu_s+\frac{5}{7}\lambda_s\right)(f-1)\mu_i-5600\mu_m\left(\frac{21}{10}\mu_s+\lambda_s\left(f+\frac{4}{5}\right)\right)\Bigg)\Bigg)\nu_m^2+14700\left(\mu_s+\frac{47}{49}\lambda_s\right)(f-1)\mu_i$$
$$-12000\mu_m\left(\frac{119}{50}\mu_s+\lambda_s\left(f+\frac{26}{25}\right)\right)\Bigg)\Bigg)\nu_i-14700\left(\mu_s+\frac{5}{7}\lambda_s\right)(f-1)\mu_i$$
$$+8400\left(\frac{119}{50}\mu_s+\lambda_s\left(f+\frac{26}{25}\right)\right)\Bigg)\Bigg)\nu_m+\Bigg(-8575\left(\mu_s+\frac{47}{49}\lambda_s\right)\left(f-\frac{16}{25}\right)\mu_i$$
$$+7000\left(\frac{42}{25}\mu_s+\lambda_s\left(f+\frac{4}{5}\right)\right)\mu_m\Bigg)\nu_i+8575\left(\mu_s+\frac{5}{7}\lambda_s\right)\left(f-\frac{16}{25}\right)\mu_i-4900\left(\frac{42}{25}\mu_s+\lambda_s\left(f+\frac{4}{5}\right)\right)\mu_m\Bigg)a$$
$$-8000\left(\nu_i-\frac{7}{10}\right)\mu_s(\mu_s+\lambda_s)\left((f-1)\nu_m^2+\left(-\frac{3}{2}f+\frac{3}{2}\right)\nu_m+\frac{7}{8}f-\frac{14}{25}\right)\Bigg),$$

$$
\begin{aligned}
\overline{\mu}_{lower}^{numer} = \\
&2000\mu_m\left(\frac{1}{2}\left(\nu_m-\frac{7}{5}\right)\left(\left(\left((\mu_i-\mu_m)\nu_i+\frac{7}{5}\mu_i+\frac{7}{10}\mu_m\right)\nu_m\right.\right.\right.\\
&\left.+\left(-\frac{7}{10}\mu_i-\frac{7}{5}\mu_m\right)\nu_i-\frac{49}{50}\mu_i+\frac{49}{50}\mu_m\right)(\mu_i-\mu_m)a^2\\
&+\left(\left(-\frac{49}{5}\left(\mu_s+\frac{47}{49}\lambda_s\right)(\mu_i-\mu_m)\nu_i+\left(\frac{49}{5}\mu_s+7\lambda_s\right)\mu_i-\frac{343}{50}\left(\mu_s+\frac{47}{49}\lambda_s\right)\mu_m\right)\nu_m\right.\\
&+\left(\left(\frac{329}{50}\lambda_s+\frac{343}{50}\mu_s\right)\mu_i-\frac{49}{5}\left(\mu_s+\frac{5}{7}\lambda_s\right)\mu_m\right)\nu_i-\frac{343}{50}\left(\mu_s+\frac{5}{7}\lambda_s\right)(\mu_i-\mu_m)a\\
&-8\left(\nu_i-\frac{7}{10}\right)\mu_s\left(\nu_m-\frac{7}{10}\right)(\mu_s+\lambda_s)f^{\frac{10}{3}}+\left(\left(\left((\mu_i-\mu_m)\nu_i+\frac{7}{5}\mu_i+\frac{7}{10}\mu_m\right)\left(\mu_i+\frac{1}{2}\mu_m\right)\nu_m^2\right.\right.\\
&-\frac{3}{2}\mu_i\left(\left(\mu_i+\frac{11}{10}\mu_m\right)\nu_i+\frac{7}{5}\mu_i+\frac{7}{10}\mu_m\right)\nu_m+\left(\frac{7}{8}\mu_i^2-\frac{49}{40}\mu_i\mu_m+\frac{7}{2}\mu_m^2\right)\nu_i\\
&+\frac{49}{40}(\mu_i+2\mu_m)(\mu_i-\mu_m)\Big)a^2+\left(\left(\left(\left(-\frac{49}{5}\mu_s-\frac{47}{5}\lambda_s\right)\mu_i-7\left(\mu_s+\frac{5}{7}\lambda_s\right)\mu_m\right)\nu_i\right.\right.\\
&+\frac{49}{5}\left(\mu_s+\frac{5}{7}\lambda_s\right)\left(\mu_i+\frac{1}{2}\mu_m\right)\Big)\nu_m^2+\left(\left(\left(\frac{147}{10}\mu_s+\frac{141}{10}\lambda_s\right)\mu_i+21\left(\mu_s+\frac{5}{7}\lambda_s\right)\mu_m\right)\nu_i\right.\\
&-\frac{147}{10}\left(\mu_s+\frac{5}{7}\lambda_s\right)(\mu_i+\mu_m)\Big)\nu_m+\left(\left(-\frac{343}{40}\mu_s-\frac{329}{40}\lambda_s\right)\mu_i-14\mu_m\left(\mu_s+\frac{1}{2}\lambda_s\right)\right)\nu_i\\
&+\left(\frac{343}{40}\mu_s+\frac{49}{8}\lambda_s\right)\mu_i+\frac{49}{5}\mu_m\left(\mu_s+\frac{1}{2}\lambda_s\right)\Big)a-8\mu_s\left(\nu_m^2-\frac{3}{2}\nu_m+\frac{7}{8}\right)\left(\nu_i-\frac{7}{10}\right)(\mu_s+\lambda_s)f^{\frac{7}{3}}\\
&+\left(-\frac{63}{100}(\mu_i-\mu_m)\left((\mu_i-8\mu_m)\nu_i+\frac{7}{5}\mu_i+\frac{28}{5}\mu_m\right)a^2+\left(-\frac{252}{25}\left(\nu_i-\frac{7}{10}\right)\mu_m\left(\mu_s+\frac{1}{2}\lambda_s\right)\nu_m\right.\right.\\
&+\left(\left(\frac{3087}{500}\mu_s+\frac{2961}{500}\lambda_s\right)\mu_i+\frac{252}{25}\mu_m\mu_s\right)\nu_i+\left(-\frac{3087}{500}\mu_s-\frac{441}{100}\lambda_s\right)\mu_i-\frac{882}{125}\mu_m\mu_s\Big)a\\
&+\frac{126}{25}\mu_s\left(\nu_i-\frac{7}{10}\right)(\mu_s+\lambda_s)f^{\frac{5}{3}}-\frac{1}{16}\left((\mu_i-8\mu_m)\nu_i+\frac{7}{5}\mu_i+\frac{28}{5}\mu_m\right)\\
&\times\left(((f+2)\mu_i-\mu_m(f-1))\nu_m^2+\frac{6}{5}\mu_i\nu_m+\left(-7f-\frac{56}{25}\right)\mu_i+7\mu_m\left(f-\frac{7}{25}\right)\right)a^2\\
&+\left(\left(\left(\frac{49}{80}(f+2)\left(\mu_s+\frac{47}{49}\lambda_s\right)\mu_i-\frac{1}{2}\left(-\frac{21}{5}\mu_s+\lambda_s\left(f-\frac{8}{5}\right)\right)\mu_m\right)\nu_i\right.\right.\\
&-\frac{49}{80}(f+2)\left(\mu_s+\frac{5}{7}\lambda_s\right)\mu_i+\frac{7}{20}\left(-\frac{21}{5}\mu_s+\lambda_s\left(f-\frac{8}{5}\right)\right)\mu_m\Big)\nu_m^2\\
&+\left(\left(\left(\frac{141}{200}\lambda_s+\frac{141}{200}\mu_s\right)\mu_i+\frac{21}{25}\mu_m\left(\mu_s+\frac{1}{7}\lambda_s\right)\nu_i+\left(-\frac{147}{200}\mu_s-\frac{21}{40}\lambda_s\right)\mu_i\right.\right.\\
&-\frac{147}{250}\mu_m\left(\mu_s+\frac{1}{7}\lambda_s\right)\Big)\nu_m+\left(-\frac{343}{80}\left(f+\frac{8}{25}\right)\left(\mu_s+\frac{47}{49}\lambda_s\right)\mu_i\right.\\
&+\frac{7}{2}\left(-\frac{21}{25}\mu_s+\lambda_s\left(f-\frac{2}{5}\right)\right)\mu_m\Big)\nu_i+\frac{343}{80}\left(f+\frac{8}{25}\right)\left(\mu_s+\frac{5}{7}\lambda_s\right)\mu_i\\
&-\frac{49}{20}\left(-\frac{21}{25}\mu_s+\lambda_s\left(f-\frac{2}{5}\right)\right)\mu_m\Big)a\\
&+\frac{1}{2}\mu_s\left((f+2)\nu_m^2+\frac{6}{5}\nu_m-7f-\frac{56}{25}\right)\left(\nu_i-\frac{7}{10}\right)(\mu_s+\lambda_s),
\end{aligned}
$$

$$
\begin{aligned}
&\overline{\mu}_{lower}^{denom} = \\
&-2000\left(\nu_m-\frac{4}{5}\right)\Bigg((\mu_i-\mu_m)\Bigg(\left((\mu_i-\mu_m)\nu_i+\frac{7}{5}\mu_i+\frac{7}{10}\mu_m\right)\nu_m+\left(-\frac{7}{10}\mu_i-\frac{7}{5}\mu_m\right)\nu_i \\
&-\frac{49}{50}\mu_i+\frac{49}{50}\mu_m\Bigg)a^2+\Bigg(\left(-\frac{49}{5}\left(\mu_s+\frac{47}{49}\lambda_s\right)(\mu_i-\mu_m)\nu_i+\left(\frac{49}{5}\mu_s+7\lambda_s\right)\mu_i\right. \\
&\left.-\frac{343}{50}\left(\mu_s+\frac{47}{49}\lambda_s\right)\mu_m\right)\nu_m+\left(\left(\frac{329}{50}\lambda_s+\frac{343}{50}\mu_s\right)\mu_i-\frac{49}{5}\left(\mu_s+\frac{5}{7}\lambda_s\right)\mu_m\right)\nu_i \\
&-\frac{343}{50}\left(\mu_s+\frac{5}{7}\lambda_s\right)\left(\mu_i-\mu_m\right)a-8\left(\nu_i-\frac{7}{10}\right)\mu_s\left(\nu_m-\frac{7}{10}\right)\left(\mu_s+\lambda_s\right)f^{\frac{10}{3}} \\
&+\Bigg(\left(2000(\mu_i-\mu_m)\nu_i+\frac{7}{5}\mu_i+\frac{7}{10}\mu_m\right)\left(\mu_i+\frac{1}{2}\mu_m\right)\nu_m^2-3000\mu_i\left(\left(\mu_i+\frac{11}{10}\mu_m\right)\nu_i+\frac{7}{5}\mu_i+\frac{7}{10}\mu_m\right)\nu_m \\
&+(1750\mu_i^2-2450\mu_i\mu_m+7000\mu_m^2)\nu_i+2450(\mu_i+2\mu_m)(\mu_i-\mu_m)\Bigg)a^2 \\
&+\Bigg(\left(\left((-19600\mu_s-18800\lambda_s)\mu_i-14000\left(\mu_s+\frac{5}{7}\lambda_s\right)\mu_m\right)\nu_i+19600\left(\mu_s+\frac{5}{7}\lambda_s\right)\left(\mu_i+\frac{1}{2}\mu_m\right)\right)\nu_m^2 \\
&+\Bigg(\left((29400\mu_s+28200\lambda_s)\mu_i+42000\left(\mu_s+\frac{5}{7}\lambda_s\right)\mu_m\right)\nu_i-29400\left(\mu_s+\frac{5}{7}\lambda_s\right)(\mu_i+\mu_m)\Bigg)\nu_m \\
&+\Bigg((-17150\mu_s-16450\lambda_s)\mu_i-28000\mu_m\left(\mu_s+\frac{1}{2}\lambda_s\right)\Bigg)\nu_i+(17150\mu_s+12250\lambda_s)\mu_i \\
&+19600\mu_m\left(\mu_s+\frac{1}{2}\lambda_s\right)\Bigg)a-16000\mu_s\left(\nu_m^2-\frac{3}{2}\nu_m+\frac{7}{8}\right)\left(\nu_i-\frac{7}{10}\right)(\mu_s+\lambda_s)f^{\frac{7}{3}} \\
&+\Bigg(-1260(\mu_i-\mu_m)\left((\mu_i-8\mu_m)\nu_i+\frac{7}{5}\mu_i+\frac{28}{5}\mu_m\right)a^2+\Bigg(-20160\left(\nu_i-\frac{7}{10}\right)\mu_m\left(\mu_s+\frac{1}{2}\lambda_s\right)\nu_m \\
&+((12348\mu_s+11844\lambda_s)\mu_i+20160\mu_m\mu_s)\nu_i+(-12348\mu_s-8820\lambda_s)\mu_i-14112\mu_m\mu_s\Bigg)a \\
&+10080\mu_s\left(\nu_i-\frac{7}{10}\right)(\mu_s+\lambda_s)f^{\frac{5}{3}}+250\Bigg(\left((f-1)\mu_i-\left(f+\frac{1}{2}\right)\mu_m\right)\nu_m^2 \\
&+\left(\left(\frac{3}{5}f-\frac{3}{5}\right)\mu_i-\frac{3}{5}f\mu_m\right)\nu_m+\left(\frac{7}{5}f+\frac{28}{25}\right)\mu_i-\frac{7}{5}\left(f-\frac{7}{10}\right)\mu_m\left(\left(\mu_i-8\mu_m\right)\nu_i+\frac{7}{5}\mu_i+\frac{28}{5}\mu_m\right)a^2 \\
&+\Bigg(\left(\left(-2450(f-1)\left(\mu_s+\frac{47}{49}\lambda_s\right)\mu_i+2000\mu_m\left(\frac{21}{10}\mu_s+\lambda_s\left(f+\frac{4}{5}\right)\right)\right)\right)\nu_i \\
&+2450\left(\mu_s+\frac{5}{7}\lambda_s\right)(f-1)\mu_i-1400\mu_m\left(\frac{21}{10}\mu_s+\lambda_s\left(f+\frac{4}{5}\right)\right)\Bigg)\Bigg)\nu_m^2 \\
&+\Bigg(\left(-1470(f-1)\left(\mu_s+\frac{47}{49}\lambda_s\right)\mu_i+1200\left(\frac{7}{5}\mu_s+\lambda_s\left(f+\frac{1}{5}\right)\right)\mu_m\right)\nu_i \\
&+1470(f-1)\left(\mu_s+\frac{5}{7}\lambda_s\right)\mu_i-840\left(\frac{7}{5}\mu_s+\lambda_s\left(f+\frac{1}{5}\right)\right)\mu_m\Bigg)\nu_m \\
&+\Bigg(-3430\left(f+\frac{4}{5}\right)\left(\mu_s+\frac{47}{49}\lambda_s\right)\mu_i+2800\left(-\frac{21}{10}\mu_s+\lambda_s(f-1)\right)\mu_m\Bigg)\nu_i \\
&+3430\left(f+\frac{4}{5}\right)\left(\mu_s+\frac{5}{7}\lambda_s\right)\mu_i-1960\left(-\frac{21}{10}\mu_s+\lambda_s(f-1)\right)\mu_m\Bigg)a \\
&-2000\mu_s\left((f-1)\nu_m^2+\left(\frac{3}{5}f-\frac{3}{5}\right)\nu_m+\frac{7}{5}f+\frac{28}{25}\right)(\mu_s+\lambda_s)\left(\nu_i-\frac{7}{10}\right).
\end{aligned}
$$

Acknowledgements

This work is funded by National Natural Science Foundation of China (No. 11702041), Natural Science Foundation of Chongqing (No. cstc2020jcyj-msxm X0097), and Fundamental Research Funds for the Central Universities (No. 2020CDJ-LHSS-005).

References

1. J.D. Eshelby, *The determination of the elastic field of an ellipsoidal inclusion, and related problems*, Proceedings of the Royal Society of London Series A – Mathematical and Physical Sciences, **241**, 376–396, 1957.
2. R. Hill, *A self-consistent mechanics of composite materials*, Journal of the Mechanics and Physics of Solids, **13**, 213–222, 1965.
3. T. Mori, K. Tanaka, *Average stress in matrix and average elastic energy of materials with misfitting inclusions*, Acta Metallurgica, **21**, 571–574, 1973.
4. M. Hori, S. Nemat-Nasser, *Double-inclusion model and overall moduli of multi-phase composites,* Mechanics of Materials, **14**, 189–206, 1993.
5. Z. Hashin, *The Elastic Moduli of Heterogeneous Materials*, Journal of Applied Mechanics, **29**, 143–150, 1962.
6. Z. Hashin, B.W. Rosen, *The elastic moduli of fiber-reinforced materials*, Journal of Applied Mechanics, **31**, 223–232, 1964.
7. Z. Hashin, S. Shtrikman, *A variational approach to the theory of the elastic behaviour of multiphase materials*, Journal of the Mechanics and Physics of Solids, **11**, 127–140, 1963.
8. Z. Hashin, *Analysis of composite materials - A survey*, Journal of Applied Mechanics, **50**, 481–505, 1983.
9. K.E. Aifantis, H. Askes, *Gradient elasticity with interfaces as surfaces of discontinuity for the strain gradient*, Journal of the Mechanical Behavior of Materials, **18**, 283–306, 2007.
10. Y. Ban, C. Mi, *On spherical nanoinhomogeneity embedded in a half-space analyzed with Steigmann–Ogden surface and interface models*, International Journal of Solids and Structures, **216**, 123–135, 2021.
11. Q.H. Fang, Y.W. Liu, B. Jin, P.H. Wen, *Interaction between a dislocation and a core-shell nanowire with interface effects*, International Journal of Solids and Structures, **46**, 1539–1546, 2009.
12. H.M. Shodja, H. Ahmadzadeh-Bakhshayesh, M.Y. Gutkin, S*ize-dependent interaction of an edge dislocation with an elliptical nano-inhomogeneity incorporating interface effects*, International Journal of Solids and Structures, **49**, 759–770, 2012.
13. M. Wang, W. Ye, *Size-dependent elastic field of nano-inhomogeneity: from interface effect to interphase effect*, Archive of Applied Mechanics, **90**, 2319–2333, 2020.
14. G. Chatzigeorgiou, F. Meraghni, A. Javili, *Generalized interfacial energy and size effects in composites*, Journal of the Mechanics and Physics of Solids, **106**, 257–282, 2017.

15. Z. HASHIN, *The spherical inclusion with imperfect interface*, Journal of Applied Mechanics, **58**, 444–449, 1991.

16. S. FIROOZ, G. CHATZIGEORGIOU, F. MERAGHNI, A. JAVILI, *Homogenization accounting for size effects in particulate composites due to general interfaces*, Mechanics of Materials, **139**, 103204, 2019.

17. S. FIROOZ, G. CHATZIGEORGIOU, F. MERAGHNI, A. JAVILI, *Bounds on size effects in composites via homogenization accounting for general interfaces*, Continuum Mechanics and Thermodynamics, **32**, 173–206, 2020.

18. R. SHUTTLEWORTH, *The surface tension of solids*, Proceedings of the Physical Society. Section A, **63**, 444, 1950.

19. M.E. GURTIN, A.I. MURDOCH, *A continuum theory of elastic material surfaces*, Archive for Rational Mechanics and Analysis, **57**, 291–323, 1975.

20. R.E. MILLER, V.B. SHENOY, *Size-dependent elastic properties of nanosized structural elements*, Nanotechnology, **11**, 139, 2000.

21. R. DINGREVILLE, J. QU, *Interfacial excess energy, excess stress and excess strain in elastic solids: planar interfaces*, Journal of the Mechanics and Physics of Solids, **56**, 1944–1954, 2008.

22. R. DINGREVILLE, J.M. QU, M. CHERKAOUI, *Surface free energy and its effect on the elastic behavior of nano-sized particles, wires and films*, Journal of the Mechanics and Physics of Solids, **53**, 1827–1854, 2005.

23. S. LI, W. YIMING, H. ZHUPING, W. JIANXIANG, *Interface effect on the effective bulk modulus of a particle-reinforced composite*, Acta Mechanica Sinica, **20**, 676–679, 2004.

24. T. CHEN, G.J. DVORAK, C.C. YU, *Solids containing spherical nano-inclusions with interface stresses: effective properties and thermal–mechanical connections*, International Journal of Solids and Structures, **44**, 941–955, 2007.

25. G.W. MILTON, S.K. SERKOV, *Neutral coated inclusions in conductivity and anti–plane elasticity*, Proceedings of the Royal Society of London, Series A: Mathematical, Physical and Engineering Sciences, **457**, 1973–1997, 2001.

26. R.M. CHRISTENSEN, K.H. LO, *Solutions for effective shear properties in three phase sphere and cylinder models*, Journal of the Mechanics and Physics of Solids, **27**, 315–330, 1979.

27. H.L. DUAN, J. WANG, Z.P. HUANG, B.L. KARIHALOO, *Size-dependent effective elastic constants of solids containing nano-inhomogeneities with interface stress*, Journal of the Mechanics and Physics of Solids, **53**, 1574–1596, 2005.

28. J. WANG, H.L. DUAN, Z. ZHANG, Z.P. HUANG, *An anti-interpenetration model and connections between interphase and interface models in particle-reinforced composites*, International Journal of Mechanical Sciences, **47**, 701–718, 2005.

29. H.L. DUAN, J. WANG, Z.P. HUANG, Z.Y. LUO, *Stress concentration tensors of inhomogeneities with interface effects*, Mechanics of Materials, **37**, 723–736, 2005.

30. H. DUAN, B. KARIHALOO, *Thermo-elastic properties of heterogeneous materials with imperfect interfaces: Generalized Levin's formula and Hill's connections*, Journal of the Mechanics and Physics of Solids, **55**, 1036–1052, 2007.

31. L.J. Walpole, *A coated inclusion in an elastic medium*, Mathematical Proceedings of the Cambridge Philosophical Society, **83**, 495–506, 1978.

32. E. Herve, A. Zaoui, *n-Layered inclusion-based micromechanical modelling*, International Journal of Engineering Science, **31**, 1–10, 1993.

33. E. Hervé-Luanco, *Elastic behaviour of multiply coated fibre-reinforced composites: simplification of the* $(n+1)$*-phase model and extension to imperfect interfaces*, International Journal of Solids and Structures, **196-197**, 10–25, 2020.

34. E. Hervé-Luanco, *Elastic behavior of composites containing multi-layer coated particles with imperfect interface bonding conditions and application to size effects and mismatch in these composites*, International Journal of Solids and Structures, **51**, 2865–2877, 2014.

35. D.-C. Pham, T.-K. Nguyen, B.-V. Tran, *Macroscopic elastic moduli of spherically-symmetric-inclusion composites and the microscopic stress-strain fields*, International Journal of Solids and Structures, **169**, 141–165, 2019.

36. D.C. Pham, T.K. Nguyen, *The microscopic conduction fields in the multi-coated sphere composites under the imposed macroscopic gradient and flux fields,* Zeitschrift für angewandte Mathematik und Physik, **70**, 24, 2019.

37. D.C. Pham, *Solutions for the conductivity of multi-coated spheres and spherically symmetric inclusion problems*, Zeitschrift für angewandte Mathematik und Physik, **69**, 13, 2018.

38. D.C. Pham, N. Phan-Thien, *Bounds and extremal elastic moduli of isotropic quasi-symmetric multicomponent materials*, International Journal of Engineering Science, **36**, 273–281, 1998.

39. D.-C. Pham, *Bounds on the effective conductivity of statistically isotropic multicomponent materials and random cell polycrystals*, Journal of the Mechanics and Physics of Solids, **59**, 497–510, 2011.

40. D.C. Pham, L.D. Vu, V.L. Nguyen, *Bounds on the ranges of the conductive and elastic properties of randomly inhomogeneous materials*, Philosophical Magazine, **93**, 2229–2249, 2013.

41. S. Firooz, P. Steinmann, A. Javili, *Homogenization of composites with extended general interfaces: comprehensive review and unified modeling*, Applied Mechanics Reviews, **73**, 2021.

42. J.D. Eshelby, *The Continuum Theory of Lattice Defects*, in: F. Seitz, D. Turnbull (Eds.) *Solid State Physics*, Academic Press, pp. 79–144, 1956.

43. Y. Benveniste, T. Miloh, *Imperfect soft and stiff interfaces in two-dimensional elasticity*, Mechanics of Materials, **33**, 309–323, 2001.

44. S. Biwa, N. Ito, N. Ohno, *Elastic properties of rubber particles in toughened PMMA: ultrasonic and micromechanical evaluation*, Mechanics of Materials, **33**, 717–728, 2001.

45. Q. Xu, K.E. Jensen, R. Boltyanskiy, R. Sarfati, R.W. Style, E.R. Dufresne, *Direct measurement of strain-dependent solid surface stress*, Nature Communications, **8**, 555, 2017.

46. Q. Xu, R.W. Style, E.R. Dufresne, *Surface elastic constants of a soft solid*, Soft Matter, **14**, 916–920, 2018.

47. R. DINGREVILLE, J. QU, *A semi-analytical method to compute surface elastic properties*, Acta Materialia, **55**, 141–147, 2007.

48. R. DINGREVILLE, J. QU, *A semi-analytical method to estimate interface elastic properties*, Computational Materials Science, **46**, 83–91, 2009.

49. C. MI, S. JUN, D.A. KOURIS, S.Y. KIM, *Atomistic calculations of interface elastic properties in noncoherent metallic bilayers*, Physical Review B, **77**, 075425, 2008.

50. V.B. SHENOY, *Atomistic calculations of elastic properties of metallic fcc crystal surfaces*, Physical Review B, **71**, 094104–094111, 2005.

51. Z. TANG, Y. CHEN, W. YE, *Calculation of surface properties of cubic and hexagonal crystals through molecular statics simulations*, Crystals, **10**, 2020.

52. W. YE, B. CHEN, *Investigation of the surface elasticity of GaN by atomistic simulations and its application to the elastic relaxation of GaN nanoisland*, Materials Letters, **141**, 245–247, 2015.

Received June 16, 2022; revised version September 07, 2022.
Published online September 22, 2022.